UNIVERSITY OF CALIFORNIA SAN DIEGO

Understanding the Assembly of an IKK Complex in Classical NF-kappaB Signaling Pathway using HDX-MS

A Thesis submitted in partial satisfaction of the requirements
for the degree Master of Science

in

Chemistry

by

William Suryajaya

Committee in charge:

Professor Gourisankar Ghosh, Chair
Professor Michael K. Gilson
Professor Wei Wang

2022

The Thesis of William Suryajaya is approved, and it is acceptable in quality and form for publication on microfilm and electronically.

University of California San Diego

2022

Dedication

I dedicate this work to my parents, who have supported me from the beginning.

Table of Contents

List of Figures

List of Abbreviations

DNA	deoxyribonucleic acid
FBS	fetal bovine serum
HDX-MS	Hydrogen-Deuterium Exchange-Mass Spectrometry
IκB	inhibitor of nuclear factor kappa B
IKK	inhibitor of nuclear factor kappa B kinase
IL-1	interleukin 1
IPTG	isopropyl -D-1 thiogalactopyranoside
KBD	kinase-binding domain
KD	kinase domain
LB	Luria broth
M	Molarity
MEF	mouse embryonic fibroblast
MW	molecular weight
MWCO	molecular weight cutoff
NaOH	sodium hydroxide
NBD	NEMO-binding domain
NEMO	NF-κB essential modulator
NF-κB	nuclear factor kappa-B
NIK	NF-κB-inducing kinase
PBS	phosphate-buffer saline
PCR	polymerase chain reaction
PIC	protease inhibitor cocktail

SDD	scaffold dimerization domain
SDS	sodium-dodecyl sulfate
Sf9	*Spodoptera frugiperda* cell line
SRR	serine-rich region
TAK1	transforming growth factor-beta-activated kinase 1
TE	tris-ethylenediaminetetraacetic acid
TNF-α	tumor necrosis factor alpha
Ub_4	Tetra-Ubiquitin
ULD	ubiquitin-like domain
X-Gal	5-bromo-4-chloro-3-indoyl-beta-D-galacto-pyronoside
ZFD	zinc finger domain

Acknowledgements

Thank you to Professor Gourisankar Ghosh for allowing me the opportunity to work in his lab. I am grateful for the patience he has had with me during my time as his student. He is always approachable and happy to talk about science. I am especially grateful that I was able to work during the COVID pandemic. I have learned a lot from working in his lab and I hope to continue to use the skills I have learned here in my future work.

Thank you to Shandy Shahabi for mentoring me in my early days of joining the lab. Thank you for taking time out of your day to teach me how to conduct research and find balance as a graduate student. Thank you for helping me with my experiments and for your continued advice in all things pertaining to graduate student life and beyond. Thank you for your tips in experimental design and for engaging in both academic and personal discussions in our shared office space.

Thank you to Professor Tom Huxford and his student Matt Mealka in providing a sample of IKK2 protein for this project. Thank you to Dr. Steven Silletti for assistance with processing of HDX-MS data and for answering my many questions on the matter. Thank you to Landon Azling for assistance in proofreading this work.

ABSTRACT OF THE THESIS

Understanding the Assembly of an IKK Complex in Classical NF-kappaB Signaling Pathway using HDX-MS

by

William Suryajaya

Master of Science in Chemistry

University of California San Diego, 2022

Professor Gourisankar Ghosh, Chair

The NF-κB signaling pathway plays a central role in immune response and normal cell function. A key regulator of the pathway is the IKK complex. Currently, understanding of the exact mechanism by which the IKK complex assembles remains incomplete. Linear ubiquitin chains alongside the IKK1, IKK2, and NEMO subunits of the complex have been well established as necessary for pathway activation. Phosphorylation of Ser^{177} and Ser^{181} on IKK2 subunits is a critical event in the activation of the complex. In efforts to understand the

recruitment of each subunit in forming an active kinase, HDX-MS was used to characterize the dynamics of a model NEMO:IKK2+Ub_4 complex. We confirmed previously established binding regions in both NEMO and IKK2. Linear Ub_4 was found to enhance NEMO:IKK2 inter-subunit interactions and induced long-range conformational changes in IKK2. One alteration to the dynamics of the kinase domain's activation loop exposed its critical serine residues. These changes support the model that activation of IKK2 can occur via trans-autophosphorylation, which requires both IKK2 and Ub_4-bound NEMO.

I. Introduction

A. NF-κB Signaling Pathway

Nuclear factor kappa B (NF-κB) refers to a family of structurally related eukaryotic transcription factors [1]. NF-κB signaling is a central pathway that regulates the expression of hundreds of effector genes involved in controlling cellular functions such as immune response, cell proliferation, and inflammation [2,3]. Since the discovery of NF-κB in 1986, research into the function and understanding of this single family of transcription factors has been extensive [4,5]. Although the activation of the signaling pathway protects organisms from a range of environmental stimuli, unregulated activity of NF-κB is implicated in various diseases like chronic inflammation and cancer [6]. Understanding how the signaling pathway proceeds mechanistically is therefore imperative in efforts to treat diseases.

NF-κB signaling has been classified into two major pathways. The canonical (classical) and non-canonical (alternative) signaling pathways are functionally distinct but related signaling modules (Fig. 1) [7]. Although these pathways proceed differently, both lead to the transcription of genes via members of the NF-κB family of proteins. Within mammals, the family consists of five members so called RelA, RelB, cRel, p50, and p52 [8]. In unstimulated cells, the NF-κB proteins are inactive and sequestered in the cytoplasm via interaction with inhibitory proteins known as I kappa Bs [9,10]. Upon stimulation (canonical), upstream signaling processes initiate activation of the IKK complex, which then phosphorylates I kappa B. This event marks I kappa B for ubiquitination and subsequent degradation by the 26S proteasome [10]. Degradation of the I kappa B inhibitory protein liberates NF-κB to translocate to the nucleus and activate target gene transcription. In the non-canonical pathway, kinase activity by NIK and IKK1 result in the phosphorylation and processing of p100 to p52, releasing a RelB/p52 dimer for nuclear

translocation and gene activation [11]. NF-κBs bind DNA as a variety of combinatorial dimeric transcription factors.

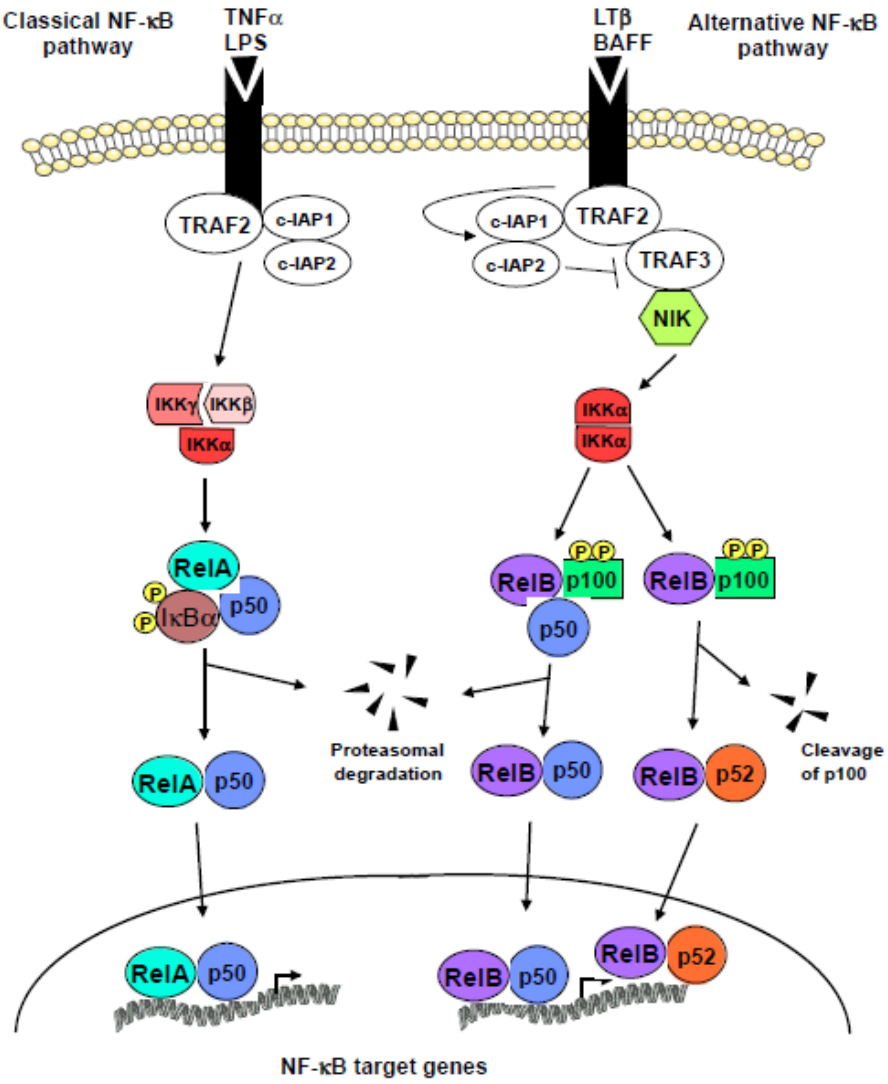

Figure 1. The classical and alternative NF-κB activation pathways. NF-κB signaling pathways comparing a TNFα/LPS-induced classical signaling pathway and a LTβ/BAFF-induced non-canonical pathway. Signaling proceeds through an IKK complex (red and pink polygons) and results in degradation of IκBα (brown oval) or processing of p100 (green rectangle) to p52 (orange circle). The outcome is nuclear translocation of NF-κB (cyan, blue, purple, and orange ovals) to the nucleus and subsequent transcription of target genes (Baud and Collares, 2016).

B. Classical IKK Signaling

Upstream signaling initiates activation of NF-κB and is tightly regulated. Although activation of the canonical signaling pathway can be initiated by different extracellular stimuli, the different modes of activation converge at a master regulator kinase complex known as the IKK complex (Fig. 2) [12]. The IKK complex controls a central event within canonical signaling, namely the phosphorylation of IκB molecules for proteasomal degradation that liberates NF-κB molecules to translocate into the nucleus and initiate transcription. A single IKK complex consists of two catalytic subunits known as IKKα/IKK1 and IKKβ/IKK2 and one regulatory subunit known as IKKγ/NEMO [13]. IKK2 is necessary for canonical signaling to occur, whereas IKK1 is primarily involved in the regulation of non-canonical signaling [14]. Gene knockout studies performed in mice also support the notion that IKK2 is primarily responsible for inducing NF-κB activity through signal-dependent phosphorylation of IκBs [15,16]. Typical illustrations of an IKK complex describe an IKK1:IKK2 heterodimer bound to NEMO. However, both IKK1 and IKK2 may function independently of each other as they have been observed to form active homodimers.

While the structurally related IKK1 and IKK2 are responsible for catalytic activity, NEMO functions as a dimeric adapter protein that mediates responses to upstream signaling molecules. IKK activation requires NEMO, but exactly how NEMO mechanistically recruits and activates IKKs remains obscure [17]. NEMO is thought to be responsible for communicating upstream signaling processes to IKK subunits. Additionally, linear ubiquitin chains are also implicated in the process of activation. Ubiquitin's role in IKK activation acts in a degradation-independent manner, which is unlike ubiquitin's role in proteasomal degradation of IκBs. Still,

the specific roles that ubiquitin and NEMO play in the activation of IKK has not been clearly established.

Within classical signaling, essential signaling events in the activation of IKK2 subunits have been identified. Activation first requires phosphorylation of two critical serine residues located in the activation loop (Ser^{177} and Ser^{181}). Phosphorylation of Ser^{177} is thought to be carried out by upstream signaling kinase TAK1, which is required for IKK activation in IL-1 and TNF stimulated MEFs [18,19]. How TAK1 is recruited to IKK2 remains unclear, although ubiquitin chains are thought to be essential in this process. Initial phosphorylation of Ser^{177} then primes IKK2 for trans-autophosphorylation of Ser^{181}, which allows IKK2 to then phosphorylate exogenous substrates. It is generally thought that ubiquitin chains help recruit upstream signaling kinases like TAK1 to phosphorylate and activate IKK2. Still, current understanding of this process does not fully explain the role that NEMO plays in IKK activation.

Perhaps the most well-studied mode of NF-κB signaling is the activation induced by tumor necrosis factor alpha (TNF-α). TNF binds to its receptor (TNFR-1) on the cell membrane, which leads to the recruitment of TRADD, cIAP1/2, and RIP1 proteins inside the cell [12, 20]. Following recruitment of these proteins, polyubiquitinated RIP1 will recruit NEMO, which is then itself ubiquitinated with M1-linked polyubiquitin chains. Ubiquitin binding of NEMO is a necessary and essential event for TNF-induced IKK activation and NF-κB activity [21]. However, it remains unclear how NEMO in conjunction with ubiquitin transmits upstream signaling events like TAK1 to IKK subunits. Previous efforts to understand the interaction between NEMO and IKK2 showed that IKK2 subunits with defective dimerization capacity failed to interact with NEMO, even though IKK2's kinase activity did not depend on

dimerization [22]. Dimerization of IKK2 subunits is necessary for its activation and ubiquitin-bound NEMO plays a critical role in this process.

It is possible then, that ubiquitin binding of NEMO initiates the activation of IKK2 by inducing conformational changes that aids in the activation of IKK2 homodimers. To initiate its own activation, these conformationally altered IKKs may then recruit other kinases such as TAK1 or other active IKKs. Higher-order complexes of IKK2 such as tetramers, hexamers, and octamers have been previously reported [23]. These higher-order complexes are thought to be physiologically significant as a platform that enables trans-autophosphorylation by placing neighboring kinase domains in local proximity. Binding of ubiquitin to NEMO may initiate formation of these higher-order complexes. As a direct result of binding to ubiquitin, changes in NEMO structure are transferred directly to IKK2 subunits via direct interaction between NEMO's N-terminal kinase binding domain (KBD) and IKK2's C-terminal NEMO binding domain (NBD). Subsequently, long-range conformational changes in IKK2 occur as a result. Efforts to understand this process previously led to the identification of a secondary site of interaction between NEMO's C-terminal region and a region preceding IKK2's NBD. These conformational changes and additional interactions likely play an essential role in enabling trans-autophosphorylation.

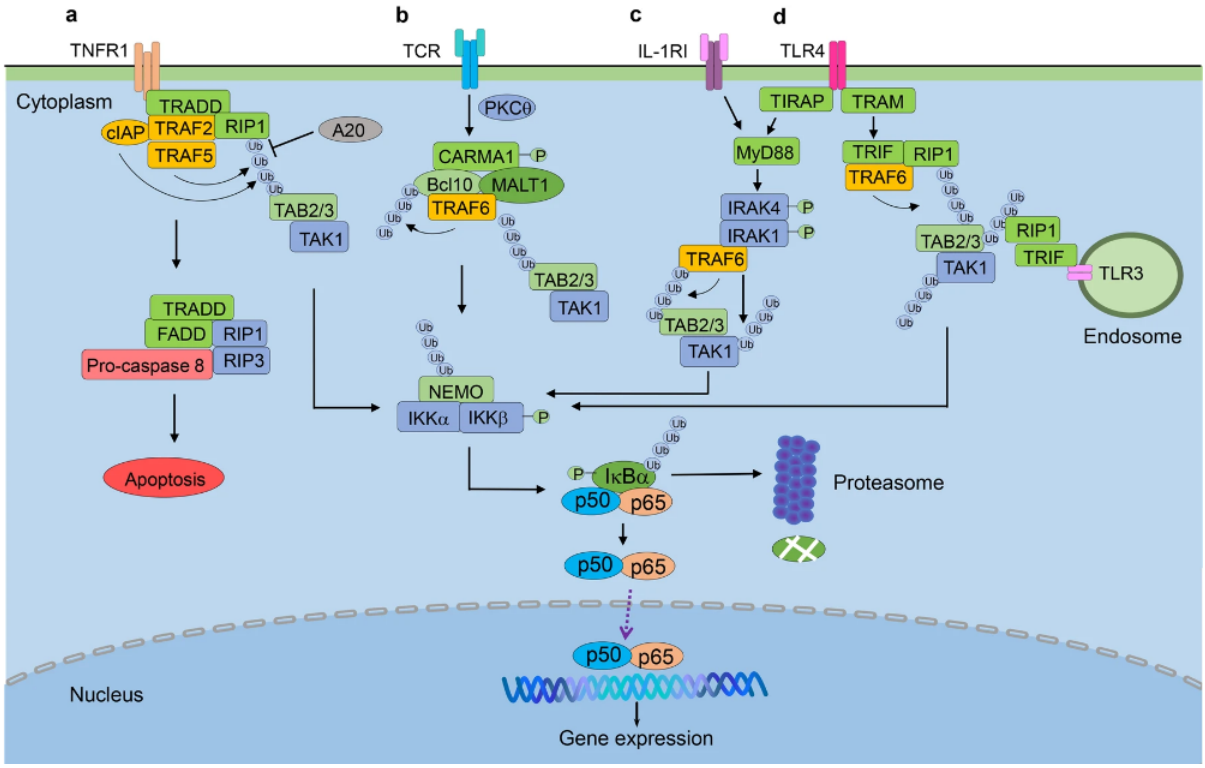

Figure 2. Activation and regulation of canonical NF-κB pathway. Canonical signaling is activated by a variety of extracellular stimuli including but not limited to TNFR1 (a), TCR (b), IL-1RI (c), and TLR4 (d). All pathways converge at the multi-subunit kinase composed of IKKα, IKKβ, and NEMO (complex shown as blue and green polygons). It is unclear how the kinase assembles, yet its function as a kinase of IκBα proteins is necessary for NF-κB activation (Yu, H., Lin, L., Zhang, Z, and Hu, H., 2020).

C. Structural Features of NEMO

Structures of both NEMO and IKK2 have been previously reported and their interacting domains have been identified (Fig. 3). Human NEMO is a 48 kDa protein that has the propensity to form higher order complexes with itself. Although the full structure of NEMO has not been characterized, NEMO adopts an elongated alpha-helical conformation. Partial crystal structures of truncated NEMO sequences and its complexes support this notion as well (Fig. 4). The 419-residue protein has three identified binding regions and a zinc finger domain (ZFD) at its C-terminus. It is pertinent to note that illustrations of the full-length protein are AlphaFold-predicted models, which were used for ease of viewing and highlighting structural features [24]. Some of these features and illustrations may not be entirely accurate to the true protein structure.

Experimentally validated crystal structures of segments of NEMO and its complexes suggest that NEMO interacts with other proteins through distinct domains (Fig. 5) [25]. The N-terminal region is uncharacterized, although a segment from residues 49-110 has been identified as the kinase binding domain (KBD). Two IKK peptides associate with two strands of NEMO, forming a heterotetramer. Two other sites of interaction that have been identified are the viral protein vFLIP binding region from residues 195-249 (vFLIP) and the ubiquitin binding domain (UBAN) from residues 259-360. This second site of interaction has been characterized as the binding domain for linear ubiquitin chains and adopts an alpha-helical secondary structure. Crystal structures of this region in complex with linear di-ubiquitin show that the ubiquitin moieties bind on the exterior surface of a dimer of NEMO UBANs, trapping the NEMO subunits together (Fig. 5D). More recent small-angle x-ray scattering experiments identified the domain spanning from KBD to vFLIP, namely residues 112-195, as essential for IKK2-induced conformational changes and signal propagation [26].

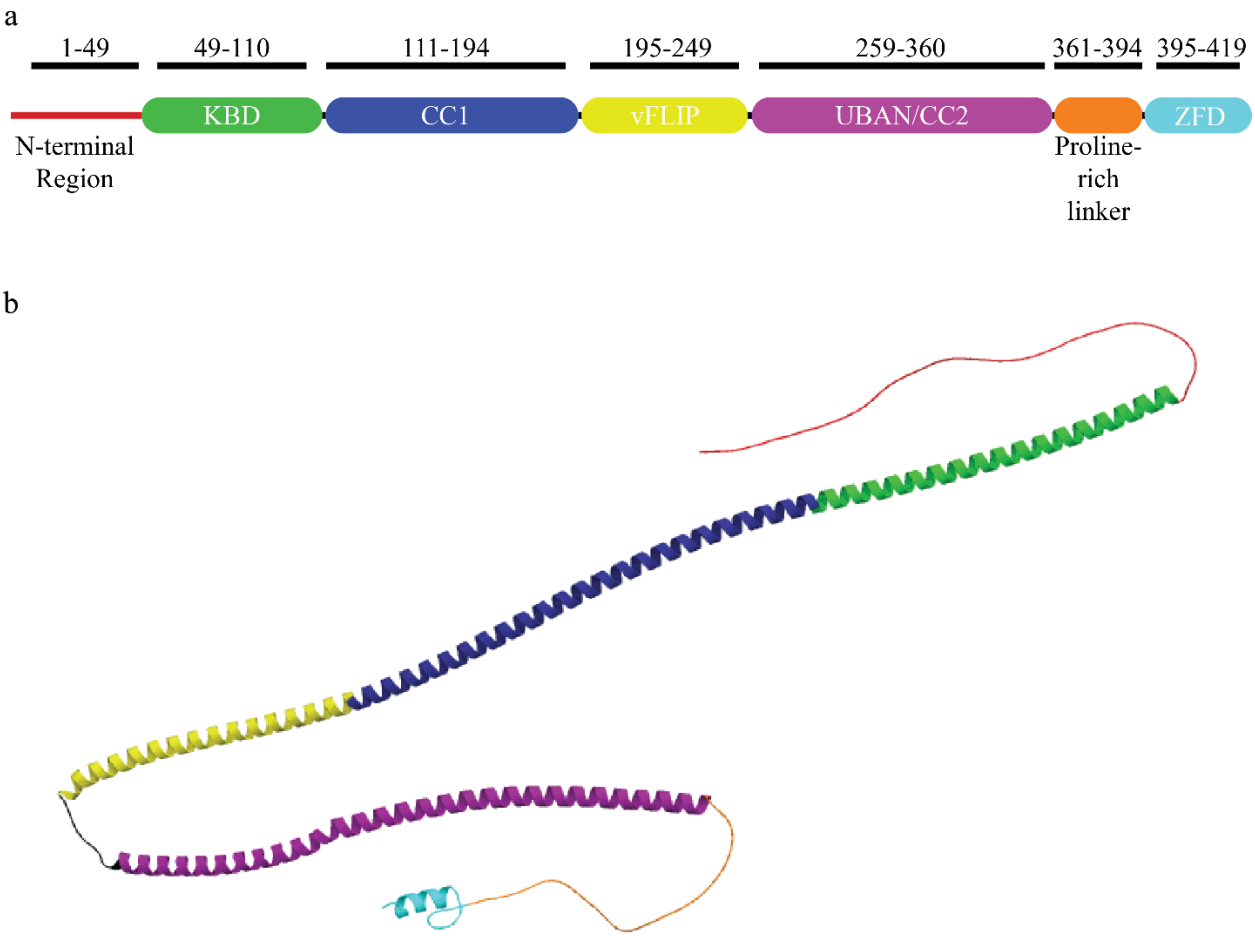

Figure 3. NEMO domain architecture and structure. NEMO exists as a long, alpha-helical protein often referred to as a coiled-coil. (A) Colored 2-dimensional domain organization of NEMO. (B) AlphaFold predicted structure of NEMO colored with the same color scheme. Three domains are known to interact and bind other proteins, namely the kinase-binding domain (KBD) which binds IKK, the vFLIP-binding domain (vFLIP), and the ubiquitin-interacting domain which is also known as the ubiquitin-binding in ABIN and NEMO motif (UBAN). The N-terminus lacks characterized secondary structure. The C-terminal Zinc finger domain (ZFD) connects to UBAN via a proline-rich segment. CC1 refers to a coiled-coil region of the protein.

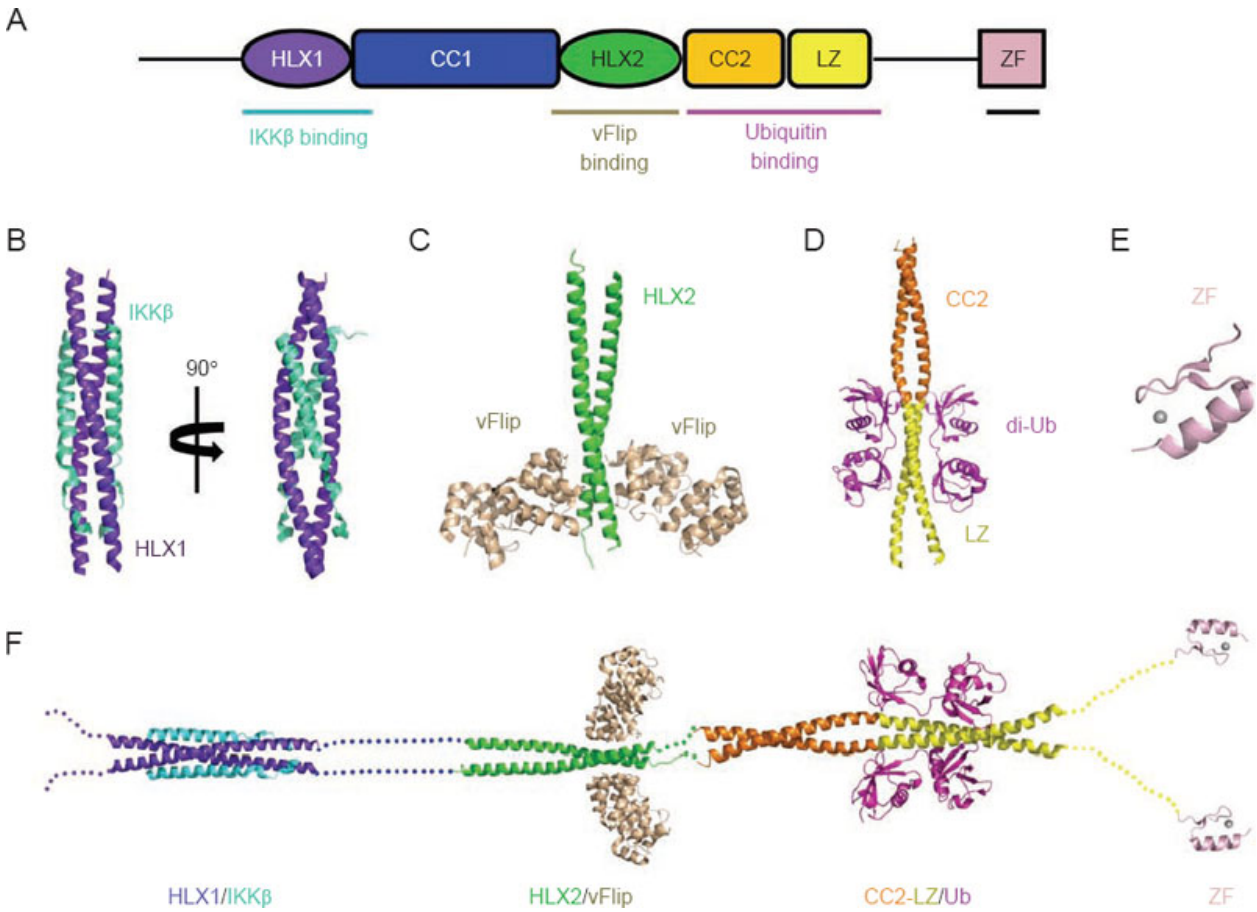

Figure 4. Structures of NEMO and their complexes. Partial crystal structures of NEMO have been reported and are summarized. (A) Domains of NEMO where HLX is a helical domain, CC is a coiled coil, LZ is a leucine zipper, and ZF is a zinc finger. (B) Structure of the NEMO kinase-binding domain in complex with an IKK2 peptide (PDB: 3BRT). (C) Structure of the NEMO HLX2 in complex with vFLIP (PDB: 3CL3). (D) Structure of murine NEMO UBAN in complex with linear di-Ub (PDB: 2ZVN). (E) Structure of the NEMO ZF (PDB: 2JVX). (F) Model of NEMO as an elongated dimer (Zheng, C., Yin, Q., and Wu, H., 2011).

D. Structural Features of IKK2

Unlike NEMO, IKK2 is a catalytic subunit of the IKK complex. Human IKK2 is a 719-residue protein with a mass of 87 kDa. The primary functional domain is its kinase domain (KD), and like other kinase domains, IKK's kinase domain shares the same structural motifs and sequence homology [27]. The protein also has a so-called ubiquitin-like domain (ULD), which makes contacts with the KD. The scaffold dimerization domain (SDD) also makes contacts with both the KD and ULD and provides a dimerization site for two IKK2 subunits. A serine-rich region (SRR) links the C-terminal end of the SDD to a relatively uncharacterized region, known as the NEMO-binding domain (NBD), which is necessary for interaction with NEMO. As previously mentioned, IKK2 subunits display a propensity for higher-order oligomerization; the most abundant form of catalytically active IKK in stimulated cells purifies as a 700-900 kDa complex. While the predominant form of IKK2 *in vitro* is the homodimer, analytical ultracentrifugation and sedimentation experiments suggest that tetramers, hexamers, and even octamers exist [23]. It is likely that these higher-order molecular weight complexes play an important physiological role. Taking these observations into account with IKK2's ability to phosphorylate other IKK2 dimers, these larger complexes may provide the necessary platform to properly orient and localize IKK2 protomers to self-activate via trans-autophosphorylation.

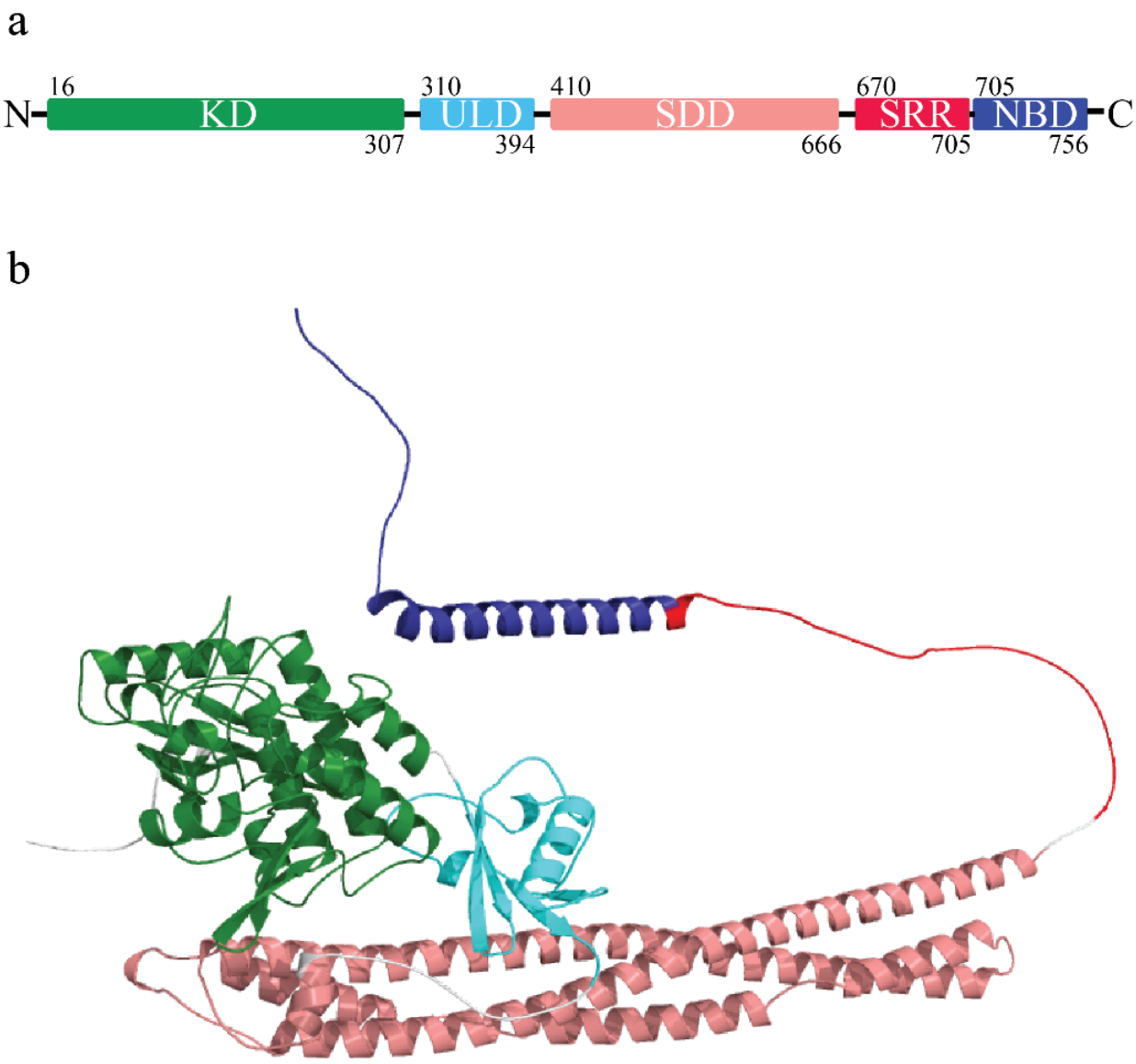

Figure 5. IKK2 domain architecture and structure. The IKK2 protein (A) Colored 2-dimensional domain organization of IKK2. (B) AlphaFold predicted structure of IKK2 colored with the same color scheme. The kinase domain (KD), ubiquitin-like domain (ULD), scaffold dimerization domain (SDD), serine-rich region (SRR), and NEMO-binding domain (NBD) are highlighted.

E. Hydrogen-Deuterium Exchange-Mass Spectrometry (HDX-MS)

In an effort to better understand how the IKK complex may assemble, I chose to use HDX-MS as a method to biophysically characterize the behavior of NEMO and IKK2 proteins *in vitro*. HDX utilizes the free exchange of protein backbone amide hydrogens with solvent deuterium ions and measures the overall incorporation of deuterium into the protein backbone. Regions which are more exposed to solvent exchange exhibit greater deuterium uptake and are considered intrinsically "disordered" and "unprotected." On the other hand, regions that show less deuterium uptake are thought to have more structure and are protected from solvent exchange. Inter-protein and intra-protein interactions further protect regions from interaction, which is an observable event in HDX data. Based on these principles, structurally dynamic regions and those involved in protein-protein or protein-ligand binding can be identified from HDX-MS data.

HDX-MS data interpretation is multifaceted and useful information can be gleaned even from spectral isotopic envelopes. Details about the interpretation of HDX-MS data are outlined [28]. Briefly, deuterium uptake over time is expected to continually increase as deuteration time increases. Spectral isotopic envelope shapes can also inform on the homogeneity of the sample as well as on possible folding/unfolding events. At its core, protein-protein interactions are expected to generate a decrease in deuterium uptake relative to the free protein. This analysis can be tricky if the protein, like IKK2 and NEMO, self-dimerize and are already in a bound state. Any additional interactions between dimers can still be detected, though the overall difference in deuterium uptake may not be obviously significant.

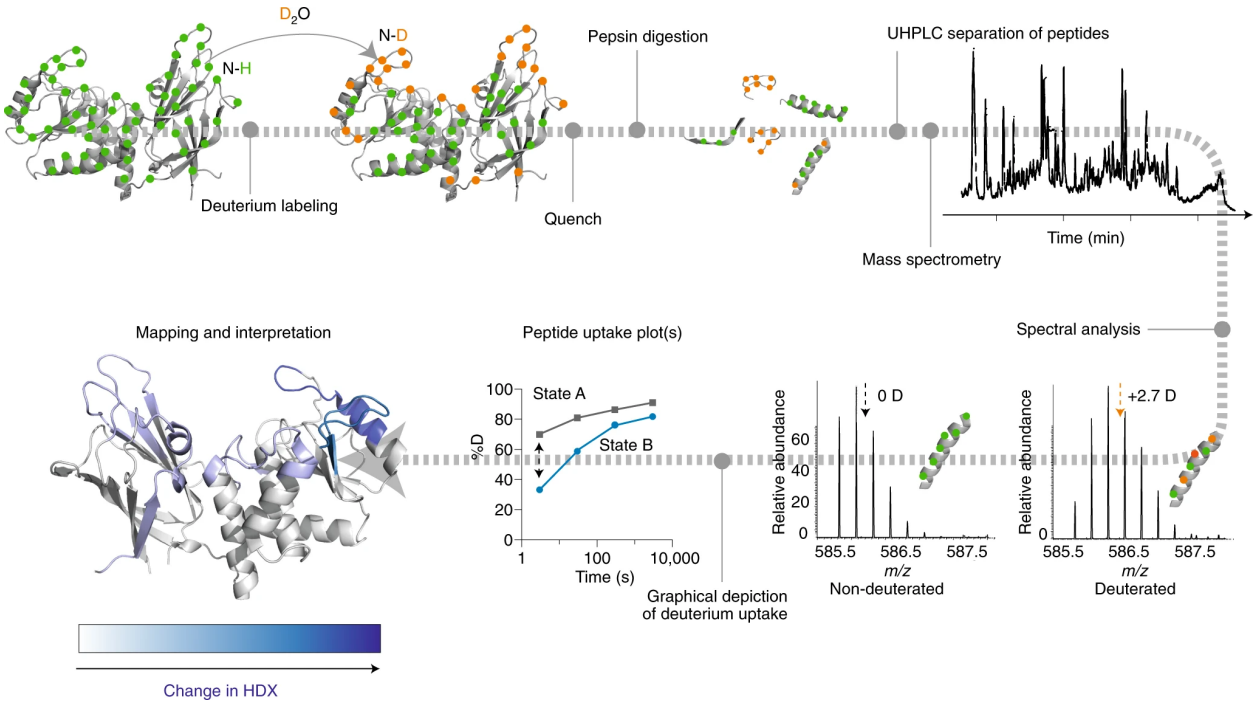

Figure 6: Schematic of HDX-MS Workflow. Proteins are first labeled in a deuterated buffer, which can be done for several timepoints and different conditions. Protein backbone amide hydrogens exchange with the solvent deuterium ions and the reaction is quenched by a drop in pH and temperature. The sample is then digested by pepsin and separated using UHPLC under cold temperatures. The process retains the deuteration state of the sample if done quickly. The sample is then eluted in a mass spectrometer, ionized, and analyzed to determine increases in mass. Intensity-weighed centroids are taken as the mass of the peptide. Differences between states can then be visualized graphically and/or mapped onto an existing structure for interpretation [29].

F. Focus of the study

The IKK-IκB-NF-κB signaling module plays an important role in cell physiology. Alterations in the spatiotemporal regulation of this module result in several human diseases. Several sub-modules within this module differ from each other via distinct members of IKK, IκB and NF-κB families which enables fine-tuning of regulatory processes. This study focuses on the kinase-level sub-module that defines the activation of p50:RelA dimer, which is guided by IKK2. In my investigation, I emphasize the dynamism of IKK2 and its modulator, NEMO. Since HDX coupled to MS is one of the most appropriate methods to study the dynamics of proteins and their complexes, I used this method to study a NEMO:IKK2 complex.

IKK2 homodimer and NEMO homodimer form a stable complex that is inactive under homeostatic conditions. Upon binding of NEMO to a linear polyubiquitin chain, IKK2 undergoes activation by phosphorylation of two serine residues located within the activation loop. It has been predicted that the coiled-coil regions of NEMO undergo conformational changes upon binding to polyubiquitin chains and transmits this signal to IKK2. I propose that binding of a tetra-ubiquitin chain (a mimic of M1-linked linear polyubiquitin chains) to NEMO induces long-range conformational changes in both NEMO and IKK2 within the NEMO:IKK2 complex, enhancing trans-autophosphorylation of IKK2. I propose that HDX-MS will help detect these changes, allow us to explain the mechanism of activation, and support a developing model of NEMO-mediated activation of IKK2.

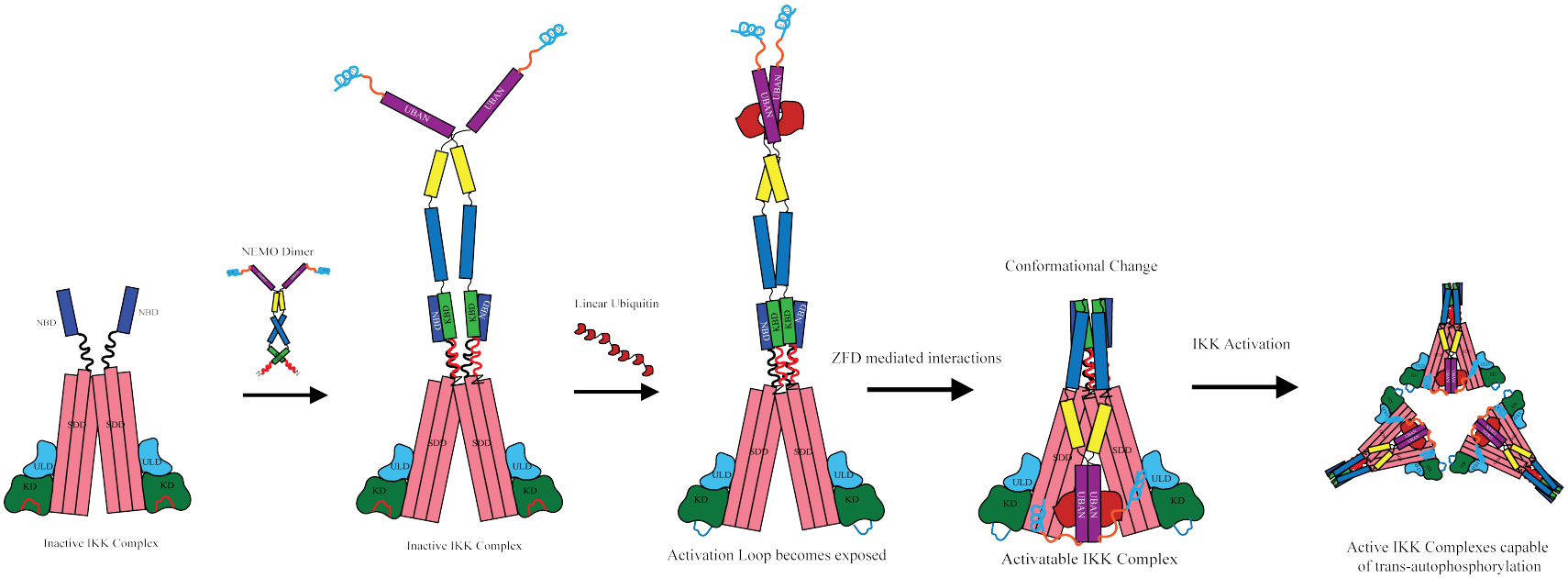

Figure 7. Proposed Model of Ub-bound NEMO anchoring and activating IKK2. Inactive IKK2 dimers bind to NEMO dimers via NBD-KBD interactions. Recruitment of linear Ub-chains to the ubiquitin-binding region (UBAN) of NEMO induces a conformational change in both NEMO and IKK2 structures, resulting in exposure of the activation loop. A C-terminal region of NEMO interacts with IKK2 away from the NBD, stabilizing the complex and enabling IKK to undergo trans-autophosphorylation.

II. Materials and Methods

A. Insect Cell Line Protein Expression

1. *Sf9* Cell Culture Techniques

Sf9 cells were cultured in complete ESF 921™ Insect Cell Culture Medium, Protein Free. Suspension cultures were maintained at a cell density of 1-4 million cells/mL at 27℃, 140 rpm. Culture volumes exceeded no more than 1/3 the flask volume. Adherent cell cultures used for baculoviral amplification were cultured in the same media as suspension cultures and maintained in a non-humidified 27°C incubator.

2. Colony Screening

His_6-IKKβ constructs were previously cloned into pFastBacHtb (Invitrogen) vector in-frame with an N-terminal hexahistidine (His_6) tag. 10 ng plasmid DNA was mixed into 50 μL chemically competent DH10 *E. coli* cells. The mixture was incubated on ice for 25 min, heat shocked at 42°C for 45 s, and placed back on ice for 2 min. 1 mL of LB supplemented with 10mM $MgCl_2$ was added to the mixture and incubated at 37°C (4 hours, 225 rpm). Cells were serially diluted and 100 μL of each dilution were plated on LB Agar plates containing 50 μg/mL Kanamycin, 7 μg /mL Gentamycin, 10 μg /mL Tetracycline, 100 μg /mL X-Gal, and 40 μg /mL IPTG (37°C, 24-48 hours, covered in foil). White colonies were selected for bacmid mini-prep and subsequent PCR confirmation.

3. Bacmid Mini-prep

2 mL overnight cultures from isolated white colonies were centrifuged at 10,000 *x g* for 30s and the supernatant was decanted. Cells were vortexed and resuspended in 100 μL of cold resuspension buffer (25 mM Tris-HCl pH 8.0, 50 mM glucose, 10 mM EDTA, 100 ug/mL RNase A). 200 μL of denaturing solution (0.2 M NaOH, 1.0% SDS) was added and the mixture inverted 10 times before putting on ice for 5 min. 150 μL of cold renaturing solution (3 M

potassium acetate, 2 M acetic acid) was added, and the mixture inverted 15 times before putting on ice for 5 min. The mixture was centrifuged (12,000 *x g*, 5 min) and the supernatant collected. 700 µL of cold 100% EtOH was added, and the solution incubated at -20°C for 30 min. The solution was centrifuged (12,000 *x g*, 30 min, 4°C). The supernatant was removed, and the pellet was washed with 500 µL 70% EtOH, centrifuged (12,000 *x g*, 5 min) and decanted. The DNA pellet was dried over 30 min and resuspended in 50 µL TE buffer (10 mM Tris-HCl pH 8, 0.1 mM EDTA).

4. PCR Confirmation

Confirmation of transposition was performed using PCR and pUC/M13 forward and reverse primers (5'-CCC AGT CAC GAC GTT GTA AAA CG-3', 5'AGC GGA TAA CAA TTT CAC ACA GG -3') according to the Bac-to-Bac Baculovirus Expression System handbook (Invitrogen). Briefly, 25 µL reactions were prepared using 100 ng of bacmid DNA and PCR reagents such that the final concentrations of each reagent were 0.2 mM dNTP mix, 1.5 mM $MgCl_2$, 1X *Taq* polymerase PCR buffer, and 0.25 µM of each primer. 1 µL of 5 units/µL *Taq* polymerase was added to the reaction mixture. PCR cycling parameters were left unmodified from the protocol. PCR products were visualized using agarose gel electrophoresis.

5. Baculoviral Amplification

Amplification of baculovirus was carried out in adherent cell cultures. Log phase *Sf9* cells were seeded in 6 well plates at $1x10^6$ cells per well in 2 mL culture medium and incubated for 1 hour at 27°C to allow time for the cells to adhere. In parallel, 1 ug bacmid DNA was added to 100 µL cell media and 6 µL cellfectin reagent (Gibco) were added to 100 µL cell media. The two mixtures were mixed and incubated (room temperature, 30 min). The DNA-lipid mixture was then mixed with an additional 800 µL cell media added dropwise to each transfection well. 5

hours post-transfection, the media was changed, and cells were incubated at 27°C for 72-96 hours to generate P1 virus.

Media containing P1 virus was then collected and centrifuged (500 *x g*, 5 min) to remove dead cells. The supernatant was harvested, supplemented with 10% heat inactivated FBS, and stored in sterile microfuge tubes at 4°C. Log phase *Sf9* cells were again seeded in 6 well plates at $1x10^6$ cells per well in 2 mL culture medium and allowed to attach for one hour at 27°C. To each well, increasing amounts of P1 virus were added ranging from 0 μL to 200 μL. Cells were incubated at for 72 hours to generate P2 virus. Media containing P2 virus was then collected from the well with ~50% live cells after 72 hours. The media was centrifuged (500 *x g*, 5 min) and the supernatant was harvested, supplemented with 10% heat inactivated FBS, and stored in sterile microfuge tubes at 4°C. Generation of P3 virus for protein expression was performed in a 30 cm dish at a seeding density of $1x10^6$ cells/mL in 30 mL of media. Cells were allowed to attach for one hour at 27°C. 300 μL of P2 virus were added to the plate and the media was collected after 72 hours.

6. Protein Expression

Expression of recombinant His-tagged IKK2 protein was done in suspension cell cultures. Log-phase *Sf9* cells were grown in sterile 1000 mL flasks to a culture volume of 300 mL with $1x10^6$ cells/mL. 3 mL of P3 virus were added to the flask (infection) and the culture was incubated (27°C, 140 rpm). 72 hours post-infection, the culture was separated into 6 aliquots of 50 mL and cells were harvested by centrifugation (3,000 *x g*, 30 min, 4°C).

7. Protein Purification

One 50 mL aliquot of pelleted cells was resuspended in 3 mL lysis buffer containing 25 mM Tris-HCl pH 7.5, 200 mM NaCl, 5% w/v glycerol, 0.1% NP-40, 0.5 mM PMSF, 5 mM β-

Me, and 15 μL (Sigma) Protease Inhibitor Cocktail. The cells were lysed by gentle sonication and the lysate was split into two separate microfuge tubes for clarification by centrifugation (15,000 *x g*, 15 min, 4°C). Each pool of lysate was added to 100 μL of pre-equilibrated Ni-NTA resin (Biobharati) and incubated under rotation: one tube was incubated for 1 hour and the other overnight (4°C). The resin was then collected via centrifugation and washed three times using 1 mL of wash buffer (25 mM Tris-HCl pH 7.5, 200 mM NaCl, 5% w/v glycerol, 0.1% NP-40, and 5 mM β-Me). Protein was eluted in 300 μL fractions using an elution buffer consisting of 25 mM Tris-HCl pH 7.5, 200 mM NaCl, 5% w/v glycerol, 0.1% NP-40, 5 mM β-Me and 250 mM imidazole. Fractions were checked using SDS-PAGE and concentration was estimated using a Bradford assay. Due to a lack of sufficient IKK2 for HDX-MS, IKK2 used in subsequent HDX-MS experiments was generously provided by the Huxford lab [30].

B. E. Coli Protein Expression

1. NEMO Expression

His_6-NEMO constructs were cloned into pET-15b plasmid. DNA was transformed into Bl21 (DE3) cells and plated on LB Agar plates containing 100 μg/mL Ampicillin. A single colony was isolated after overnight growth and inoculated into 5-15 mL of LB/Ampicillin media. Saturated starter cultures were then added to a 1 L culture of LB/Ampicillin media and grown (at 37°C) to OD_{600}=0.2, induced with 0.2 mM IPTG, and grown overnight for 16 hours at 22°C, 150 RPM. Cells were harvested by centrifugation at 3,000 *x g* for 10 min (Beckman Coulter) and stored at -80°C.

2. NEMO Purification

Bl21 (DE3) cell pellets of His_6-NEMO constructs from 1 L cultures were resuspended in 200 mL lysis buffer (20 mM Tris-HCl pH 8.0, 300 mM NaCl, 10% w/v glycerol, 10 mM

Imidazole, 0.2% Triton X-100, 1 mM PMSF, 5 mM β-Me, 100 μL Sigma Protease Inhibitor Cocktail). Cells were lysed by sonication (VWR Scientific) and the lysate clarified twice by centrifugation at 18,000 *x g* (30 min, 4°C). The lysate was mixed with a slurry of pre-equilibrated Ni-NTA agarose resin and left at 4°C for 3 hours rotating. Nickel beads were pelleted via centrifugation and washed with 3 times with 200 mL wash buffer (same as lysis buffer). Resin-bound protein was then eluted using lysis buffer containing 250 mM imidazole and fractions were collected and checked via SDS-PAGE. Concentrations of peak fractions were determined using a Bradford assay.

3. Tetra-Ubiquitin Expression

His_6-Ub_4 constructs were cloned into pET-24d plasmid. DNA was transformed into Bl21 (DE3) cells and plated on LB Agar plates containing 100 μg/mL kanamycin. A single colony was isolated after overnight growth and inoculated into 5-15 mL of LB/kanamycin media. Saturated starter cultures were then added to a 1 L culture of LB/kanamycin media and grown (at 37°C) to OD_{600}=0.3, induced with 0.5 mM IPTG, and grown overnight for 17 hours at 16°C, 150 RPM. Cells were harvested by centrifugation at 3,000 *x g* for 10 min (Beckman Coulter) and stored at -80°C.

4. Tetra-Ubiquitin Purification

Bl21 (DE3) Cell pellets of His_6-Ub_4 constructs from 1 L cultures were resuspended in 200 mL lysis buffer (20 mM Tris-HCl pH 8.0, 500 mM NaCl, 5% w/v glycerol, 20 mM Imidazole, 0.05% Triton X-100, 1 mM PMSF, 3 mM β-Me, 100 μL Sigma Protease Inhibitor Cocktail). Cells were lysed by sonication (VWR Scientific) and the lysate clarified twice by centrifugation at 18,000 *x g* (30 min, 4°C). The lysate was mixed with a slurry of pre-equilibrated Ni-NTA agarose resin and left at 4°C for 3 hours rotating. Nickel beads were

pelleted via centrifugation and washed with 200 mL lysis buffer without PIC for a total of 3 washes. Resin-bound protein was then eluted using lysis buffer containing 300 mM imidazole. Fractions were checked using SDS-PAGE and concentrations were estimated using a Bradford assay. Peak fractions containing pure protein were collected and stored at -80°C.

C. Sample Preparation for HDX-MS

1. Apo Protein and Ub_4 Preparation in Superose6 5/150 increase column

Proteins used in HDX-MS experiments were purified using a Nickel column and then passed through a size-exclusion chromatography column. For IKK2, a sample provided by the Huxford lab was used (see Fig. 13). NEMO and Ub_4 were purified and prepared as described previously. All proteins were then buffer exchanged following the manufacturer's instructions using a BioRad NGC and Superose6 5/150 increase column into HDX buffer (300 mM NaCl, 25 mM Tris pH 8.0, 5% glycerol, 10 mM β-Me). 100 µL of protein was used for each run and peak fractions for each protein were collected and concentrated using protein concentrators (Sartorius, Vivaspin, 30,000 MWCO). Due to the limited size of sample injection, multiple runs of size-exclusion chromatography were performed to obtain enough concentrated sample (300 µL of ~30 µM samples). For apo runs of IKK2 and NEMO, proteins were diluted to a final concentration of 10 µM in HDX buffer and used as is. For samples utilizing Ub_4, a threefold molar excess of Ub_4 was used relative to the protein of interest. IKK2 was mixed with Ub_4 such that the final concentration of IKK2 was 10 µM and the final concentration of Ub_4 was 30 µM. NEMO was mixed with Ub_4 such that the final concentration of NEMO was 10 µM and the final concentration of Ub_4 was 30 µM.

2. Complex Isolation and Preparation in Superose6 5/150 increase column

To isolate the IKK2:NEMO complex, equimolar concentrated IKK2 and concentrated NEMO samples were mixed and passed through a Superose6 gl/150 increase column in the same manner as apo proteins. Peak fractions of the IKK2:NEMO complex were collected, pooled, and concentrated as done previously. The complex was used at a final concentration of 5 μM for HDX-MS of the IKK2:NEMO sample. For HDX-MS of the IKK2:NEMO+Ub_4 sample, a final concentration of 9 μM Ub_4 was used with a 3 μM IKK2/NEMO complex.

D. Hydrogen-Deuterium Exchange Mass Spectrometry

1. HDX-MS

HDX-MS was performed at the Biomolecular and Proteomics Mass Spectrometry Facility (BPMSF) of the University California San Diego, using a Waters Synapt G2Si system with HDX technology (Waters Corporation) as described previously [31]. Deuterium exchange reactions were performed using a Leap HDX PAL autosampler (Leap Technologies, Carrboro, NC). D_2O buffer was prepared by lyophilizing buffers initially dissolved in ultrapure water and redissolving the powder in the same volume of 99.96% D_2O (Cambridge Isotope Laboratories, Inc., Andover, MA) immediately before use. Buffer composition was 300 mM NaCl, 25 mM Tris pH 8.0, 5% glycerol, and 10 mM β-Me. Triplicate measurements were made for each deuteration timepoint measured (0.5, 1, 2, and 5 min). For each reaction, 4 μL of protein was held at 25 °C for 5 min before mixing with 56 μL of D_2O buffer. The reaction was quenched for 1 min at 1°C by combining 50 μL of the reaction with 50 μL of 3M guanidine hydrochloride, final pH 2.66. The quenched sample (90 μL) was then injected in a 100 μL sample loop, followed by digestion on an in-line pepsin column (Immobilized Pepsin, Pierce) at 15°C. The resulting peptides were captured on a BEH C18 Vanguard precolumn, separated by analytical

chromatography (Acquity UPLC BEH C18, 1.7 µm 1.0 × 50 mm, Waters Corporation) using a 7–85% acetonitrile gradient in 0.1% formic acid over 7.5 min, and electrosprayed into the Waters Synapt G2Si quadrupole time-of-flight mass spectrometer. The mass spectrometer was set to collect data in the Mobility, ESI+ mode; mass acquisition range of 200–2000 (m/z); scan time 0.4 s. Continuous lock mass correction was accomplished with infusion of leu-enkephalin (m/z = 556.277) every 30 s (mass accuracy of 1 ppm for calibration standard).

For peptide identification, the mass spectrometer was set to collect data in mobility-enhanced data-independent acquisition (MS^E), mobility ESI+ mode instead. Peptide masses were identified from triplicate analyses and data were analyzed using the ProteinLynx global server (PLGS) version 3.0 (Waters Corporation). Peptide masses were identified using a minimum number of 250 ion counts for low energy peptides and 50 ion counts for their fragment ions; the peptides also had to be larger than 1,500 Da. The following cutoffs were used to filter peptide sequence matches: minimum products per amino acid of 0.2, minimum score of 7, maximum MH+ error of 5 ppm, and a retention time RSD of 5%. In addition, the peptides had to be present in two of the three ID runs collected. The peptides identified in PLGS were then analyzed using DynamX 3.0 data analysis software (Waters Corporation). The relative deuterium uptake for each peptide was calculated by comparing the centroids of the mass envelopes of the deuterated samples with the undeuterated controls following previously published methods [32]. For all HDX-MS data, 1 biological replicate was analyzed with 3 technical replicates. Two additional biological replicates were performed prior for apo NEMO, and 1 additional biological replicate was performed prior for NEMO+Ub_4. Data represented from different biological replicates in these cases are noted in their corresponding figures. All data are represented as mean values +/- SEM of 3 technical replicates due to processing software limitations; however, the LEAP robot

provides highly reproducible data for biological replicates. The deuterium uptake was corrected for back-exchange using a global back exchange correction factor determined from the average percent exchange measured in disordered regions of each protein [33].

E. Data Visualization

1. Uptake Plots

Deuterium uptake plots were generated in DECA (github.com/komiveslab/DECA) [34].

2. Woods Plots

Woods plots were generated in Deuteros 2.0 (github.com/andymlau/Deuteros_2.0) using data from DynamX 3.0 before back-exchange correction was applied [35].

3. Structure Figures

PDB-formatted AlphaFold computed structure were used in representing protein models (PDB IDs: AF-Q9Y6K9-F1, AF-O14920-F1) [36]. Figures depicting protein structures were generated in PyMol and colored by scripts generated either in DECA or Deuteros 2. [37]. Figures were arranged and manipulated in Adobe Illustrator [38].

III. Results

A. Expression of His-IKK2 WT FL in Insect Cell Lines

HDX-MS requires proteins and protein complexes that are both pure and of sufficient concentration to achieve reliable signals. Modern mass spectrometers can detect picomolar ion signals using only a few microliters of sample; micromolar concentrations are therefore sufficient for these experiments. IKK2, NEMO, and Ub_4 proteins were first expressed and purified as detailed in the materials and methods section. Unlike NEMO and Ub_4, IKK2 was expressed in baculovirus-infected *Sf9* cells. Steps used to make the IKK2 expression construct, its expression, and purification are described below.

Blue-white colony screening was used to distinguish clonal isolates of potential candidates containing recombinant bacmid. Figure 8 shows *DH10Bac* colonies on a LB/Agar plate following transformation of the pFastBacHtb-IKK2 vector. White colonies may possess recombinant bacmids containing the IKK2 gene if transposition has disrupted the LacZ peptide responsible for the blue phenotype, whereas blue colonies contain unaltered bacmid. White colony-derived bacmids were assessed by PCR analysis. Figure 9 shows a schematic for the transposition of the donor plasmid transposable element into the bacmid DNA with the pUC/M13 forward and reverse primers' binding sites. Using these primers, PCR can be used to confirm if the correct transposition event has occurred based on the size of the PCR product.

Figure 10 shows an agarose gel of PCR products performed on five white colonies and one blue colony. A ~4800 bp product is seen in all white colony lanes, indicating successful transposition of the IKK2 gene-carrying element into the bacmid in all five cases. It is pertinent to note that the fifth white colony did not possess contaminating bands as in the other four white colonies. Prepared bacmid should be as pure as possible for transfection. The negative control of empty bacmid is observed at ~300 bp from a blue colony, further insuring the analytical check

for transposition. *Sf9* cells are then transfected with the recombinant bacmid to produce baculovirus for protein expression and purification.

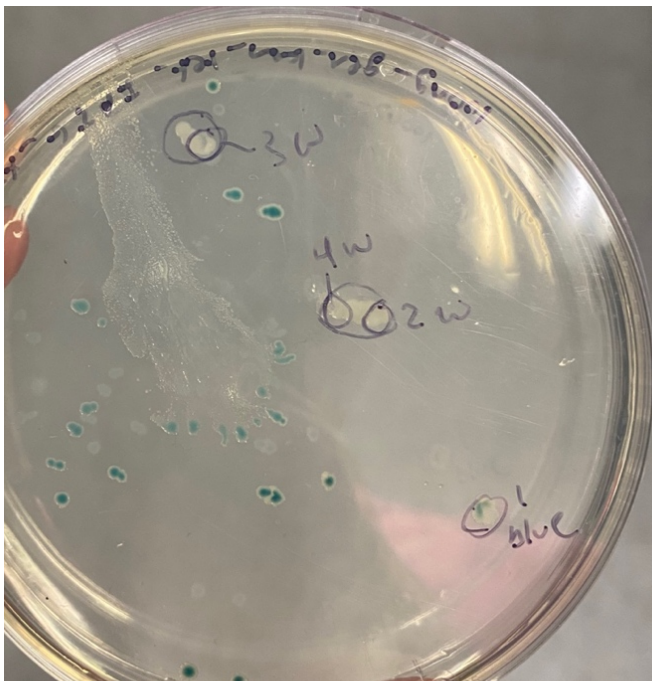

Figure 8. Blue-white colony screening for recombinant IKK2 bacmid. Transformation of pFastBacHTb-IKK2 into DH10 E. coli cells results in white colonies if the DH10 bacmid is disrupted by transposition of the insert sequence. Transposition of pFastBacHtb carrying the IKK2 gene into the DH10 bacmid generates a recombinant bacmid that is used to infect Sf9 cells and generate baculovirus for IKK2 expression in Sf9. Only white colonies of bacteria are possible candidates for recombinant bacmid.

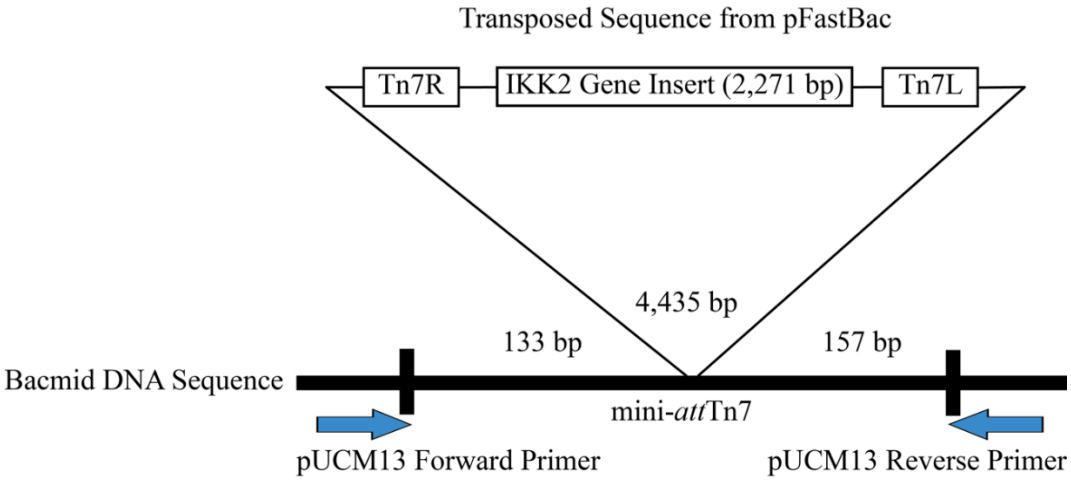

Figure 9. Analysis of recombinant bacmid DNA by PCR. The pUC/M13 forward and reverse primers bind outside of the transposition site on the bacmid DNA. PCR analysis of bacmids yields predictable PCR product sizes that depend on the size of the transposed sequence (see Table 1).

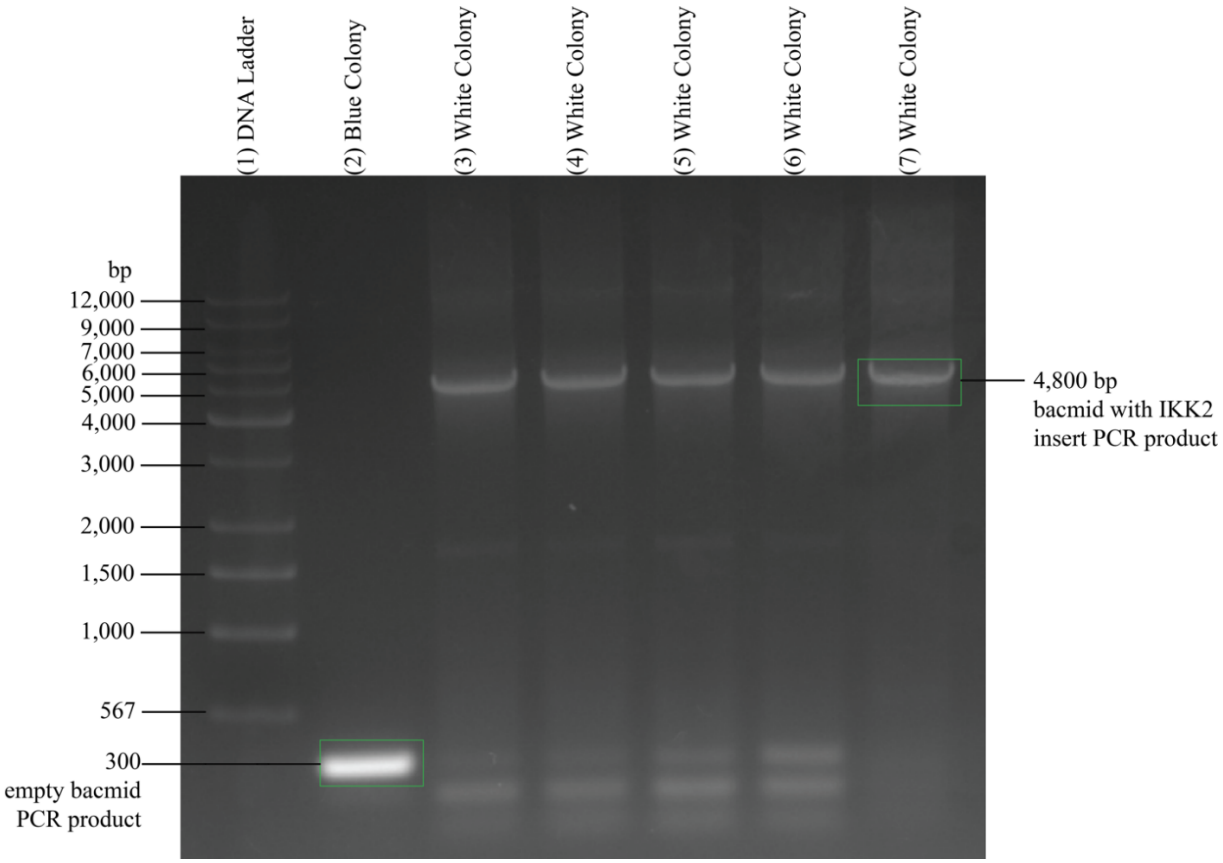

Figure 10. PCR confirmation of IKK2 gene insertion into bacmid. Successful transposition of the IKK2 gene into DH10Bac bacmid is confirmed by PCR with pUC/M13 forward and reverse primers. Use of pUC/M13 primers with Bac-to-Bac (Invitrogen) expression vectors should yield a product totaling ~2430 bp + the size of insert. In this case, His-IKK2 encoding sequence is ~2400 bp so the total PCR product size for positive confirmation is ~4800 bp. Without transposition, the PCR product of an empty bacmid is ~300 bp.

B. Purification of His-tagged IKK2, NEMO, and Ub_4

Following protein expression in *Sf9* and *E. coli*, cells were collected and lysed to release His_6-tagged proteins, which were then purified using Nickel-NTA affinity chromatography. Protein purity was checked via SDS-PAGE and concentrations of peak fractions were estimated using a Bradford assay. The following sections describe the initial purification processes for each protein prior to size-exclusion chromatography. IKK2 samples used in subsequent HDX-MS experiments provided by the Huxford Lab were purified in a similar manner and outlined below.

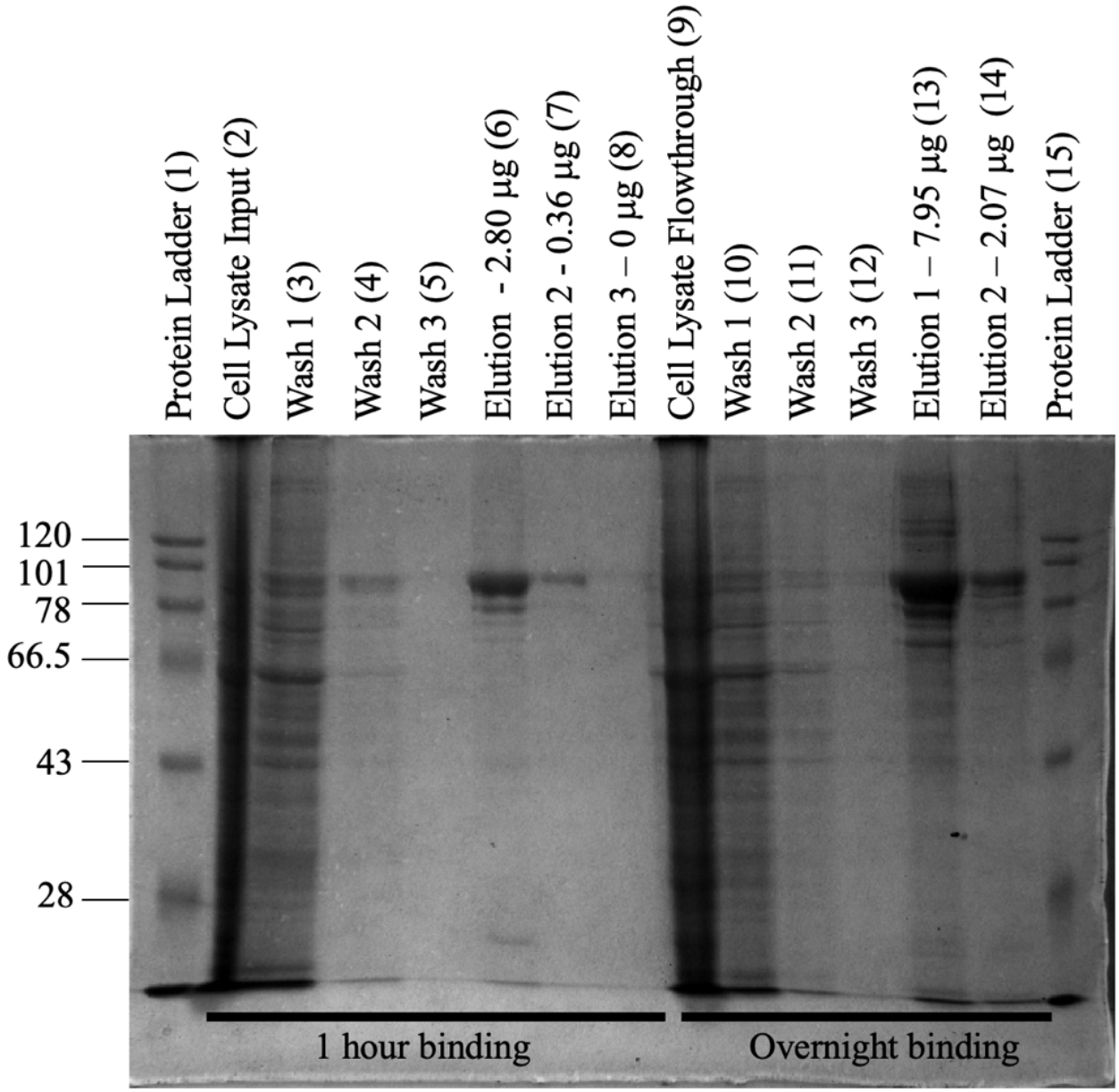

Figure 11. His_6-IKK2 Purification from Sf9 cells. His-IKK2 was purified in-house using in-batch Nickel-NTA affinity chromatography. Lanes 1 and 15 show Biobharati protein marker. Lane 2 shows 3 µL of the cell lysate input. Lanes 3-5 and lanes 10-12 all show 12 µL loads of the 3 sequential washes performed for 1-hour and overnight binding experiments, respectively. Lanes 6-8 show 12 µL of each of the 3 sequential elution fractions for the 1-hour binding experiment. Bradford assay measured concentrations for these fractions 2.68, 0.35, and 0.00 µM. Lane 9 shows 3 µL of flowthrough from the overnight binding experiment (1 hour binding flowthrough not shown due to lane limitations). Lanes 13-14 show 12 µL each of the two elution fractions for the overnight binding experiments with concentrations of 7.62 and 1.99 µM, respectively.

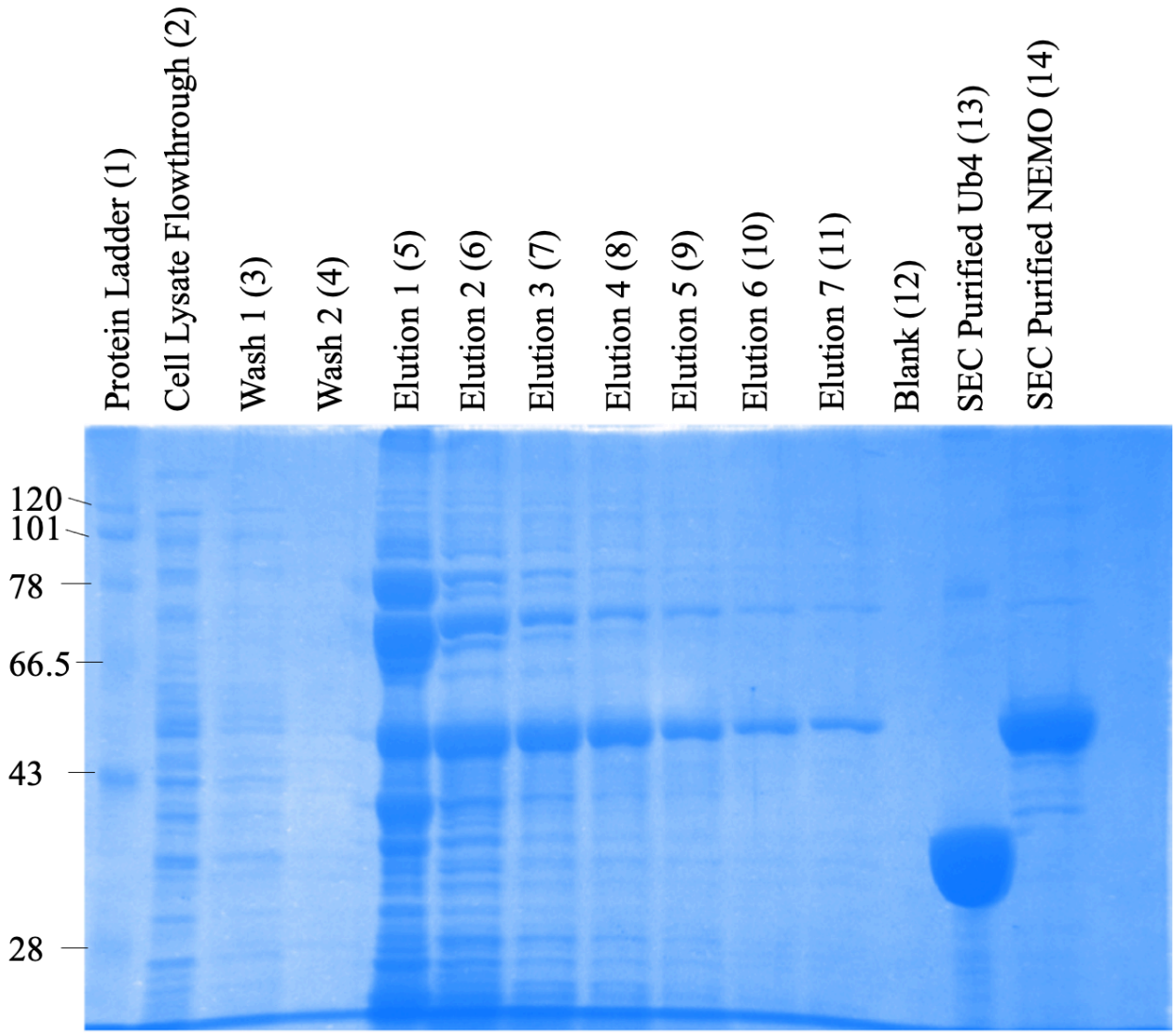

Figure 12. SDS-PAGE of full-length wild type His-NEMO purification and pooled Ub$_4$. NEMO protein was expressed in E. coli and purified using a Nickel-NTA affinity chromatography step. Lane 1 shows 1 µL of Biobharati protein ladder, lane 2 shows the flowthrough following Nickel-NTA chromatography (2 µL), lane 3-4 shows sequential washes (12 µL), lanes 5-11 show the 7 elution fractions (12 µL), and the final 2 lanes show purified controls (2 µL). SEC-purified Ub4 (5 micrograms) used for HDX-MS experiments is shown in lane 13 and a previously Nickel-purified NEMO (2 micrograms) is shown in lane 14.

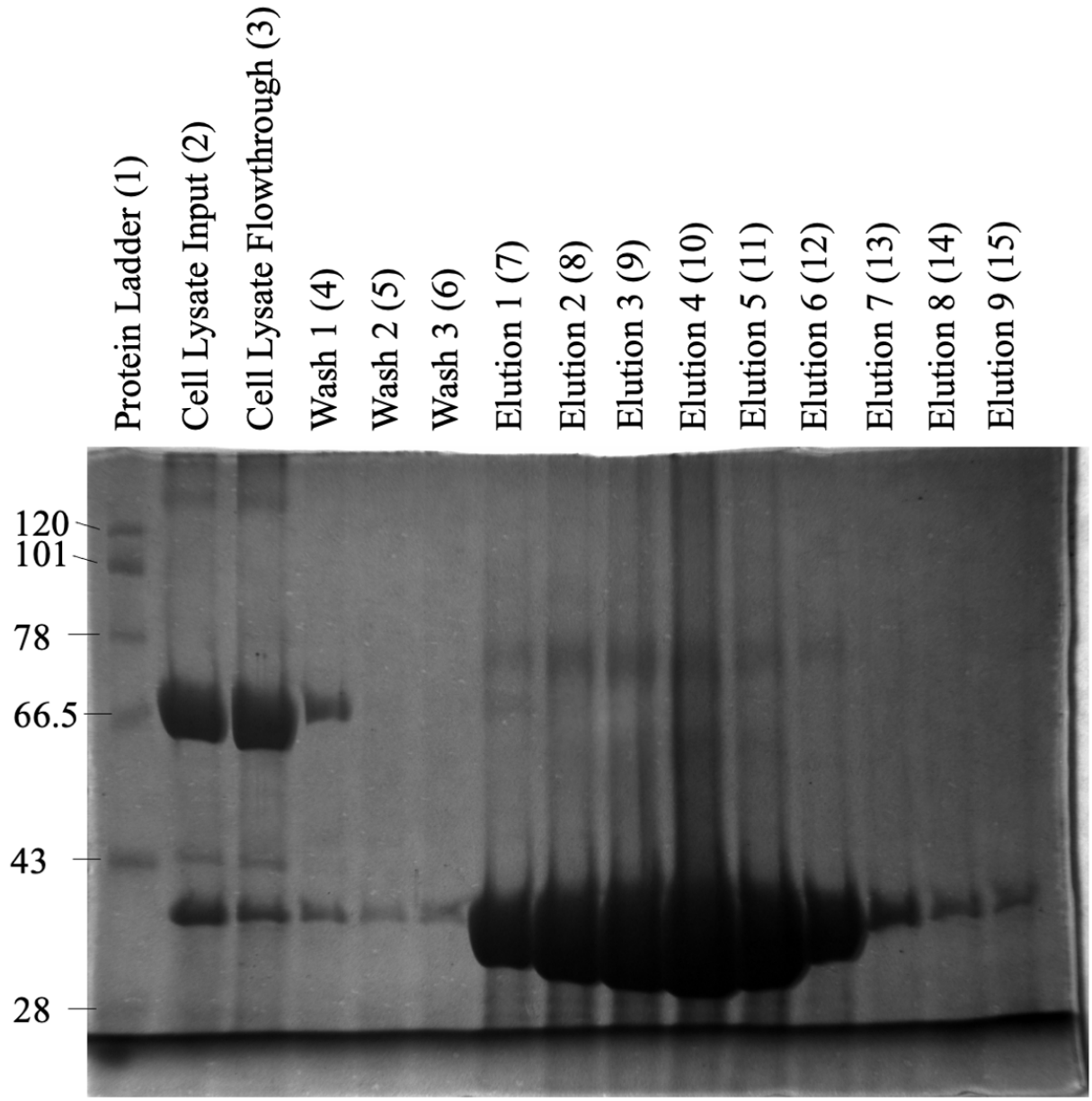

Figure 13. His_6-Ub_4 Purification from *E. coli*. His-tagged Ub4 was expressed in E. coli and purified using Nickel-NTA chromatography. Lane 1 shows 2 μL of Biobharati protein ladder, lane 2 shows the cell lysate (2 μL), lane 3 shows the cell lysate flowthrough (2 μL), lane 4-6 shows sequential washes (12 μL), and lanes 7-15 show the 9 elution fractions (12 μL). Elution fraction concentrations were measured using a Bradford assay. In order, elution fraction concentrations were measured to be 3.43, 3.68, 4.09, 4.86, 4.66, 3.25, 0.42, 0.16, and 0.09 mg/mL.

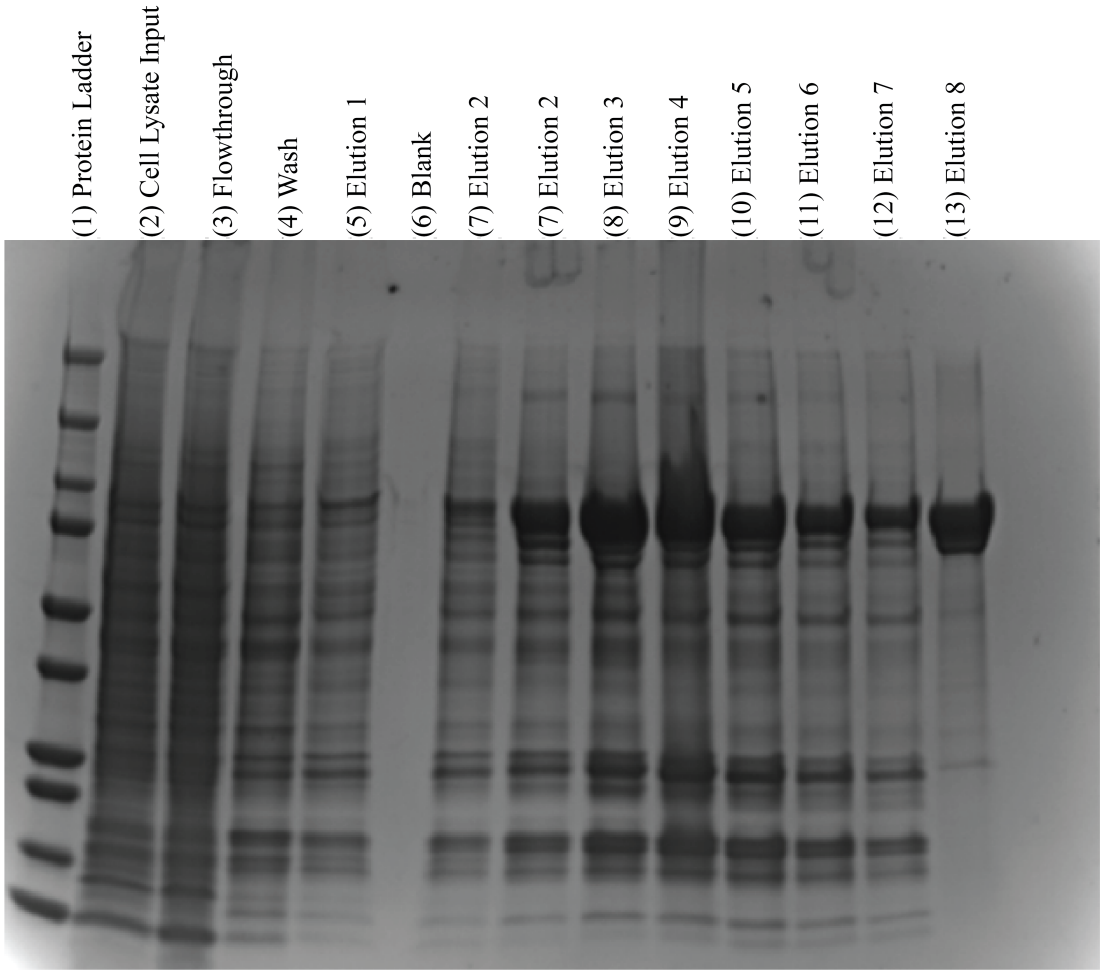

Figure 14. SDS-PAGE of His-IKK2 provided by the Huxford Lab. IKK2 provided by the Huxford lab was purified according to the protocol cited in the materials and methods. Lane 1 shows a generic protein ladder. Lanes 2 and 3 show the cell lysate input and flowthrough, respectively. Lane 4 shows a wash fraction. Lanes 5-13 show the sequential elution fractions with a blank loaded in lane 6. Lane 14 shows a previously purified IKK2 used as an additional. Size exclusion chromatography was performed on elution fractions 4, 5, and 6. Fractions 2, 3, 7, and 8 were pooled together but not used for HDX.

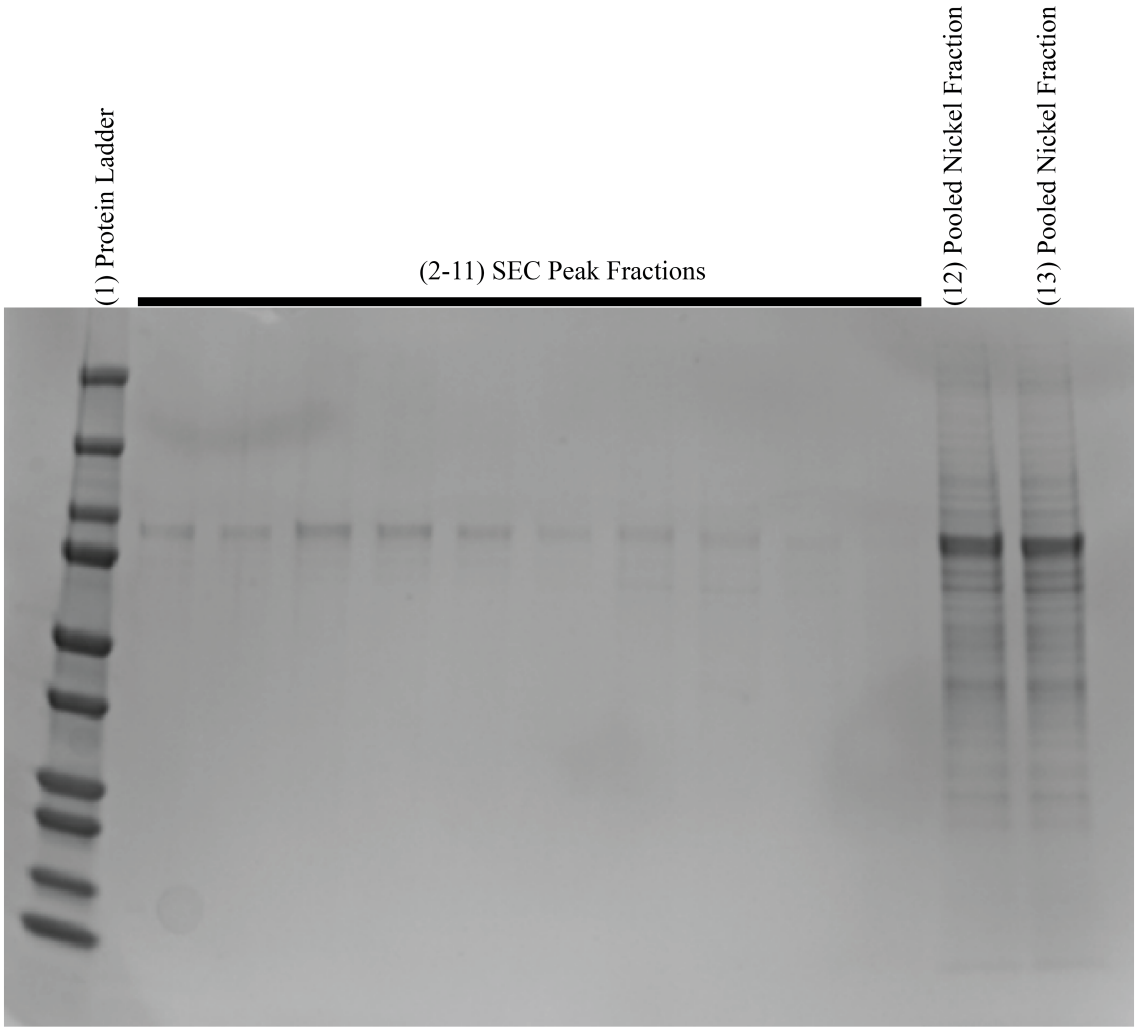

Figure 15. SDS-PAGE of SEC-purified IKK2 provided by the Huxford Lab. Following Nickel purification, IKK2 was further purified by size-exclusion chromatography. Sequential fractions covering the chromatographic peak were loaded onto an SDS-PAGE gel and the previously pooled fractions from the Nickel purification are loaded into the final two lanes as a reference. Peak fractions shown here were pooled and used for HDX-MS.

C. Sample Preparation using Size-Exclusion Chromatography

Sample preparation for HDX-MS experiments where only one protein is being studied is straightforward; pure protein can be used for the apo state and then an excess of a binding agent (small molecule, ligand, or protein) known to bind the protein of interest can be used in the bound state. Since both IKK2 and NEMO are of interest in this study, HDX-MS was performed on purified IKK2 and purified NEMO separately to generate an understanding of each protein's apo dynamism and behavior. HDX-MS was then applied on an isolated complex of IKK2:NEMO and peptides were analyzed for both proteins separately from one experiment to study the effect of oligomerization. Because both proteins have a propensity to form homodimers, it is important to consider HDX data in the context of this behavior. In an effort to gain insight on the oligomerization state of each complex, size-exclusion chromatography was performed with a BioRad protein standard and a calibration curve was made to estimate apparent molecular weights. It is essential that the isolated complexes are pure to avoid multiple populations of a protein state, which would complicate the results and provide an inaccurate apparent deuterium incorporation. The experiment was designed so that IKK2, NEMO, and an IKK2:NEMO complex were pure, isolated, and performed as separate runs. Ub_4 was then added in a 3-fold molar excess to each species for an additional three runs. The following sections describe the preparation of these samples for HDX-MS.

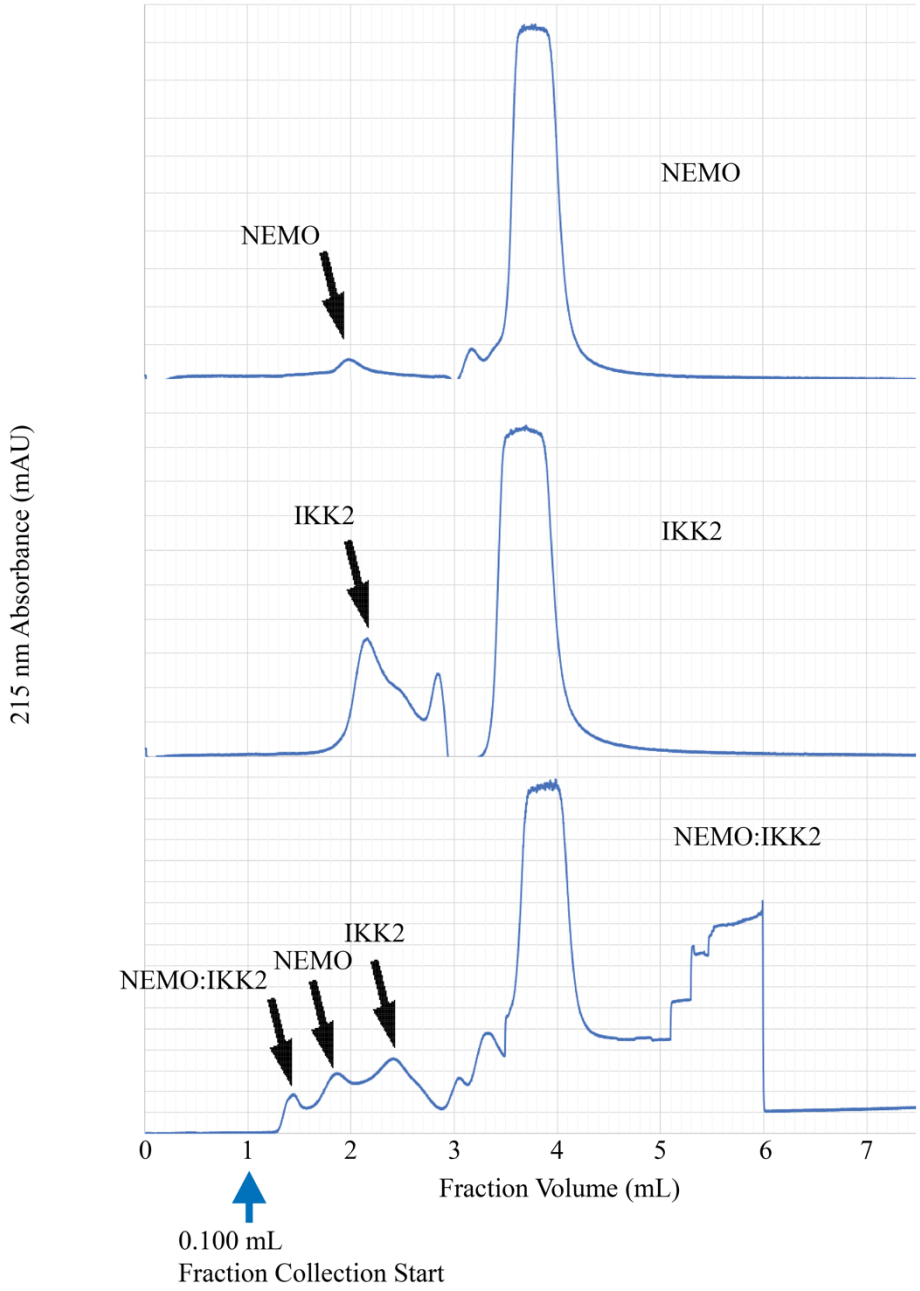

Figure 16. Superose6 5/150 increase size-exclusion chromatography chromatogram. NEMO was injected into a Superose6 5/150 increase size-exclusion column and the 215 nm elution profile was plotted (top chromatogram). IKK2 was separately injected into the same column and the chromatographic profile was plotted (middle chromatogram). A third injection of nearly equimolar IKK2 and NEMO mixture with a slight excess of the former was then injected into the column and the chromatographic profile was plotted (bottom curve). The elution profiles were assessed for purity of the isolated complex; IKK2 eluted around 2.2 mL (Fraction #12-14), NEMO eluted around 1.9 mL (Fraction #8-10), and an apparent IKK2:NEMO complex eluted around 1.4 mL (Fraction #4-6).

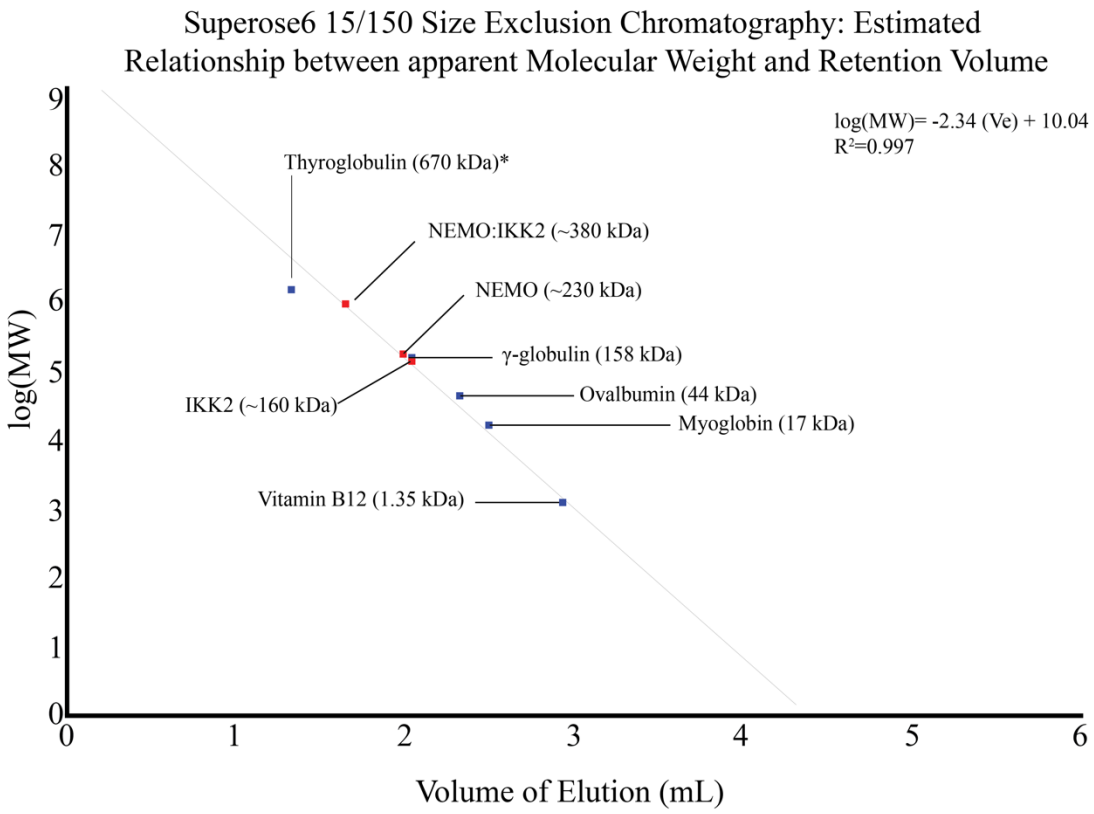

Figure 17: Superose6 5/150 increase apparent Molecular Weight. BioRad protein standard containing thyroglobulin, γ-globulin, ovalbumin, myoglobin, and vitamin B12 was injected into a Superose6 15/150 column. Peak elution volumes were identified and the log(MW) of each standard was plotted against the elution volume. Apparent molecular weights of IKK2, NEMO, and NEMO:IKK2 were calculated based on the best fit line generated from γ-globulin, ovalbumin, myoglobin, and vitamin B12.

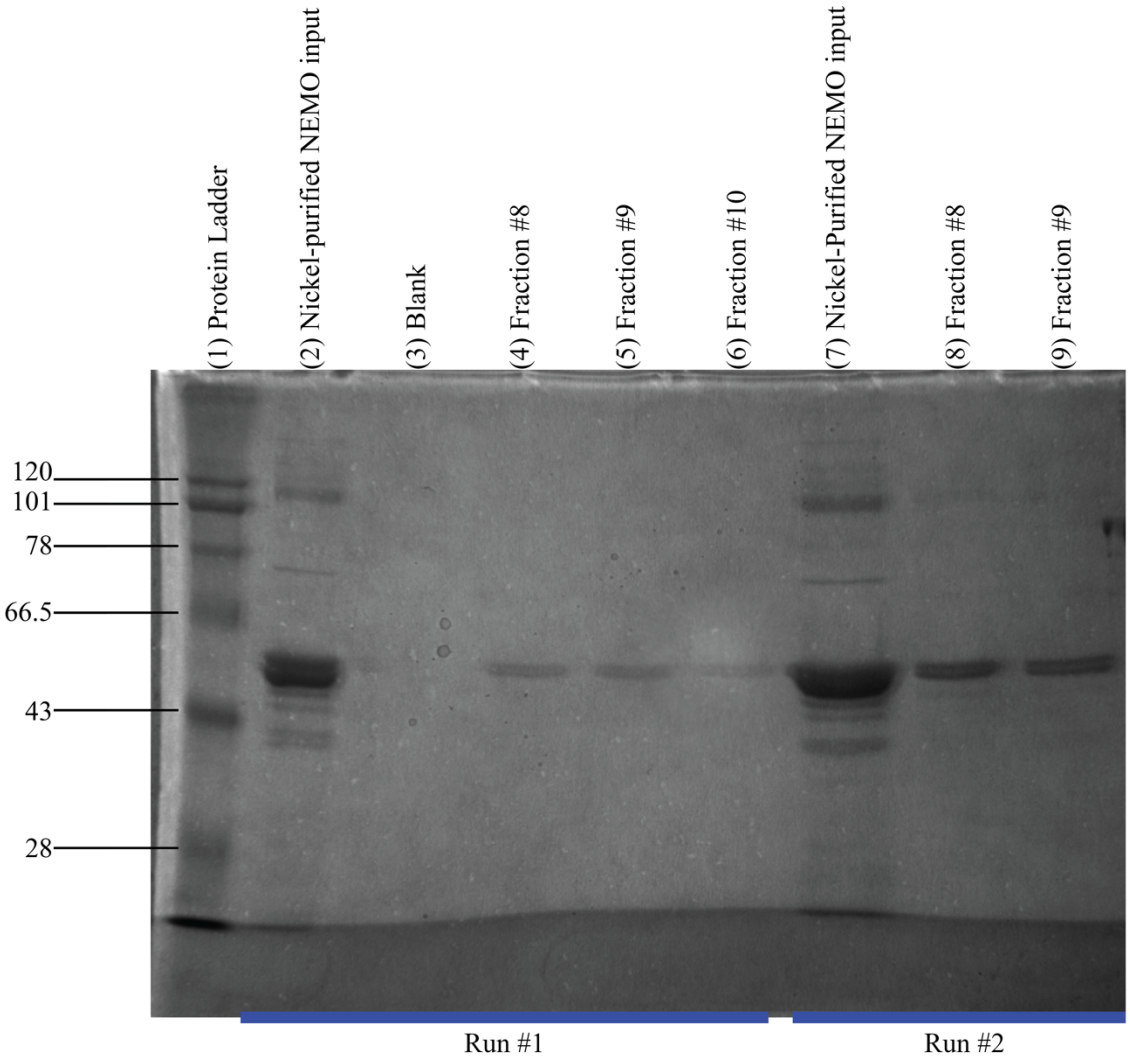

Figure 18. SDS-PAGE of size-exclusion chromatography purified NEMO. NEMO protein eluted from SEC was checked via SDS-PAGE for purity. Two separate runs are shown above with 6 μL of peak fractions loaded into each lane. Peak fraction concentrations were checked via Bradford assay and ranged from 2-3 μM. Nickel-purified inputs were ~17 μM.

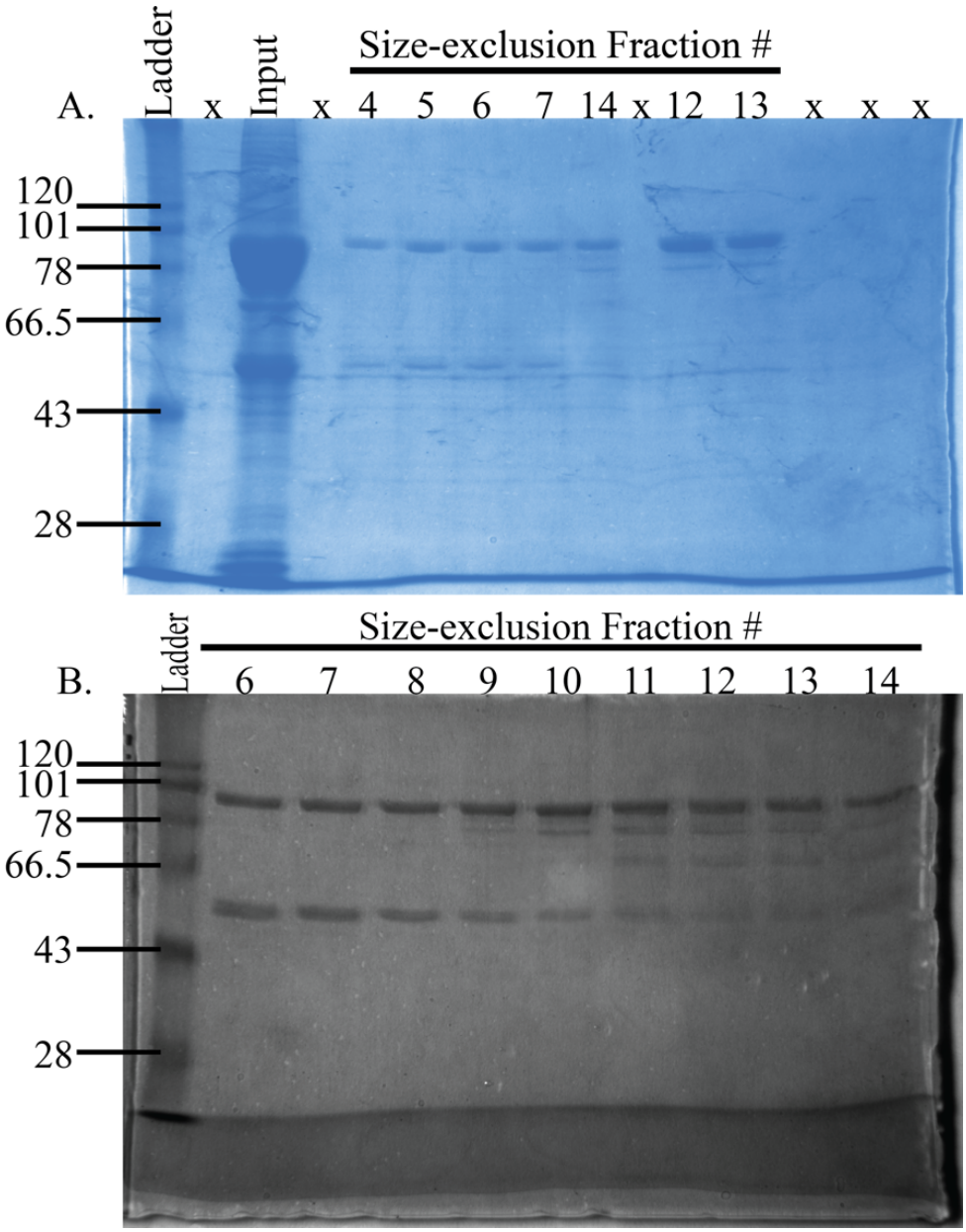

Figure 19. SDS-PAGE of SEC Peak Fractions of IKK2 and NEMO:IKK2 Complex. Nearly equimolar inputs of IKK2 and NEMO (with a slight excess of IKK2) were loaded onto the SEC column and peak fractions were checked via SDS-PAGE. Two separate runs are shown in the figures above. Figure 18a shows the initial input in lane 3 and apparent peak fractions of the complex in lanes 5-8. Peak fractions centered around the apo IKK2 elution volume were also loaded in lanes 9, 11, and 12 from this run. Figure 18b shows a second run and peak fractions ranging from the apparent IKK2:NEMO complex through the elution volumes corresponding to apo NEMO and apo IKK2.

Size-exclusion chromatography and isolation of oligomeric complexes:

IKK2, NEMO, and a NEMO:IKK2 mixture were injected into a Superose 6 15/150 size exclusion column and eluted using a BioRad NGC. IKK2 protein was observed to elute after 2.1 mL, NEMO eluted just before 2.0 mL, and the NEMO:IKK2 complex eluted around 1.5 mL based on the 215 nm chromatogram (Fig. 16). A calibration curve was made for the column using BioRad protein standard and the apparent molecular weight of each complex was calculated (Fig. 17). The results suggest that NEMO behaves as a ~230 kDa protein, IKK2 behaves like a ~160 kDa protein, and the apparent NEMO:IKK2 complex behaves as a ~380 kDa complex. Canonically, monomeric NEMO is ~48 kDa and monomeric IKK2 is ~87 kDa. Interestingly, NEMO elutes at a higher apparent MW than IKK2, likely due to interactions with the column and a non-globular shape. Because NEMO tends to adopt a highly elongated shape, this observation is consistent with previous works that suggest NEMO behaves aberrantly in solution [39, 40]. Based on these findings, it is likely that both proteins predominantly adopt a dimeric conformational state under these conditions, although other oligomeric states may also exist and have been reported before. Because the NEMO:IKK2 complex isolated elutes at an apparent molecular weight of ~380 kDa, it is likely that one NEMO dimer is interacting with one IKK2 dimer, forming a heterotetramer.

SDS-PAGE of elution peaks (Fig. 19a) shows that the first peak fraction contains both IKK2 and NEMO, confirming an oligomeric complex. Interestingly, small amounts of IKK2 can be seen co-eluting with NEMO even across the fraction ranges corresponding to apo NEMO, suggesting that NEMO's propensity for oligomerization with IKK2 can occur across multiple combinations of oligomeric states, as IKK2 does not elute in the 1.7-2.0 mL volume range (Fig. 19b). Large peaks are observed to elute after 3 mL, which are most likely imidazole and other

small molecules in the buffer. The chromatograms suggest that IKK2 and NEMO form a stable, higher molecular weight complex that is pure enough to be used for subsequent experiments. To avoid having multiple populations of oligomeric states, fractions only from the earliest elution peak were pooled and concentrated for HDX-MS.

D. HDX-MS of NEMO

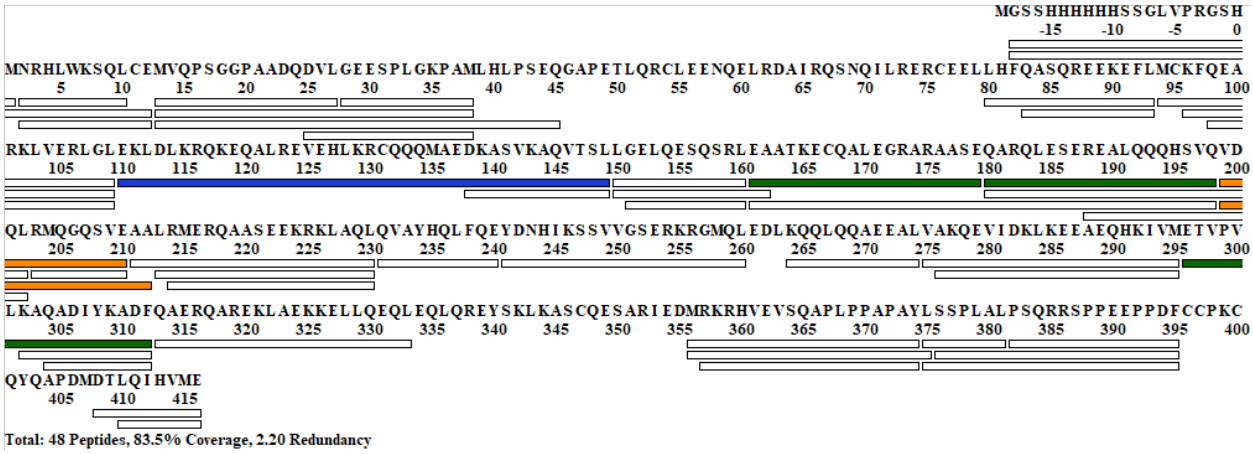

Figure 20. Peptide Coverage Map of NEMO. All peptides analyzed covered 83.5% of the overall sequence. White peptides were detected for all four states (apo NEMO, NEMO:IKK2, NEMO+Ub4, and NEMO:IKK2+Ub4). A blue peptide from residues 110-149 was not detected for the NEMO+Ub4 state but detected in all other states. Peptides colored in green were not detectable for the NEMO:IKK2 state or NEMO:IKK2+Ub4 state. Orange peptides were detected in all cases except for the NEMO:IKK2+Ub4 state.

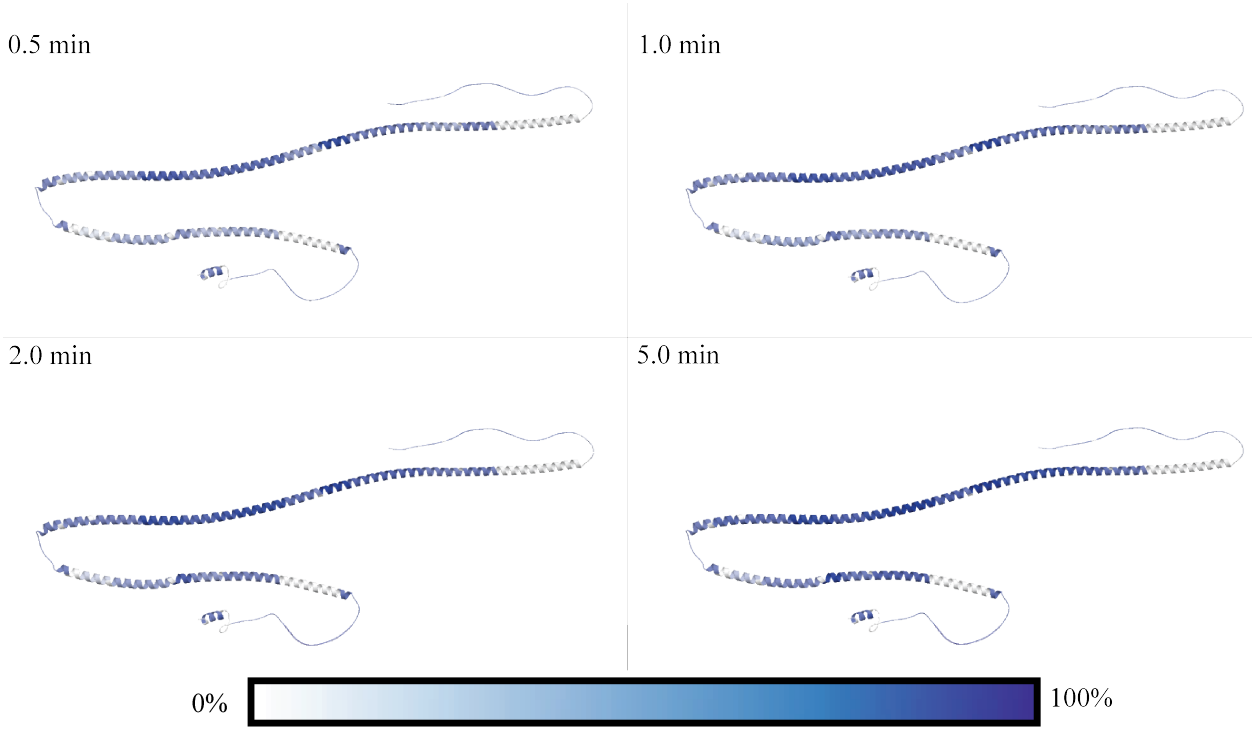

Figure 21. Apo NEMO HDX. The incorporation of deuterium across NEMO protein is mapped onto a structure using a full-range scale of percent deuterium uptake. Data from all four timepoints are separately shown in each quadrant and denoted by labeling time. Regions are colored by a gradient where increasing intensity of blue coloring indicates greater deuterium incorporation.

NEMO is a highly flexible molecule that dimerizes

Under the experimental conditions used, NEMO showed relatively high deuterium incorporation, suggesting that NEMO is a very flexible and dynamic protein. Most of the protein incorporates more than half of the maximum possible uptake within 2 minutes of deuteration time. Both the N-terminal and C-terminal domains along with a stretch of the protein spanning the C-terminal end of CC1 and the first few residues on the N-terminal side of the vFLIP binding domain exhibit high flexibility, incorporating deuterium ions rapidly within thirty seconds. The ZFD appears to have high HDX as well, suggesting that it is uninvolved in dimerization or oligomerization of NEMO subunits. One region that does not follow this trend is UBAN, which is the binding domain for linear Ub-chains. In particular, the N-terminal portion of UBAN exhibited less deuterium uptake than the rest of the protein. Although the C-terminal portion of UBAN is nearly saturated by the 5-minute timepoint, the N-terminal half remains resistant to HDX. It is possible that this site is largely responsible for the dimerization of NEMO coils, causing it to resist deuterium exchange by "masking" the backbone hydrogens via interaction with another NEMO molecule. Strikingly, NEMO shows an alternating pattern of short stretches with slight protection from deuterium uptake followed by slightly longer stretches with high exposure and HDX in a consistent manner across all four timepoints. It is likely that the regions in which NEMO is less prone to HDX are sites of interaction between two NEMO molecules used for dimerization while the regions that exhibit high HDX are non-interacting regions. These observations would be consistent with previous reports of NEMO monomers coiling together to form a NEMO dimer and higher order molecular weight assemblies.

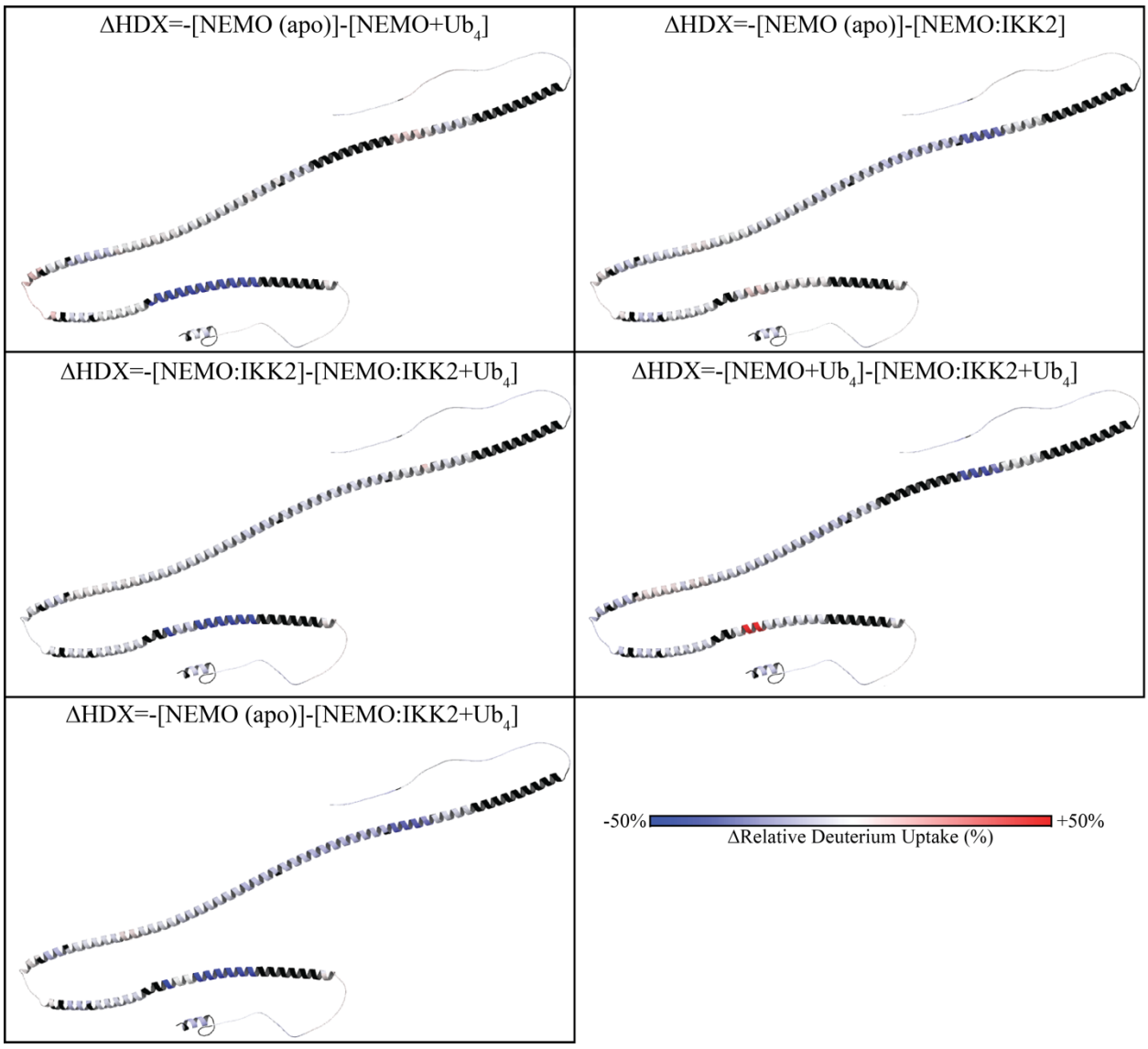

Figure 22. Differential HDX of NEMO at 5-minute timepoint. Differences in deuterium uptake between two experimental conditions (states) are mapped onto NEMO structures as ΔHDX = - [State 1] - [State 2]. To maintain a consistency with other illustrations, regions that are colored blue are those in which deuterium uptake in state 2 is less than that of state 1, indicating a protective effect. Regions that are white are non-different between the two states and regions that are red have greater deuterium incorporation in state 2 than in state 1.

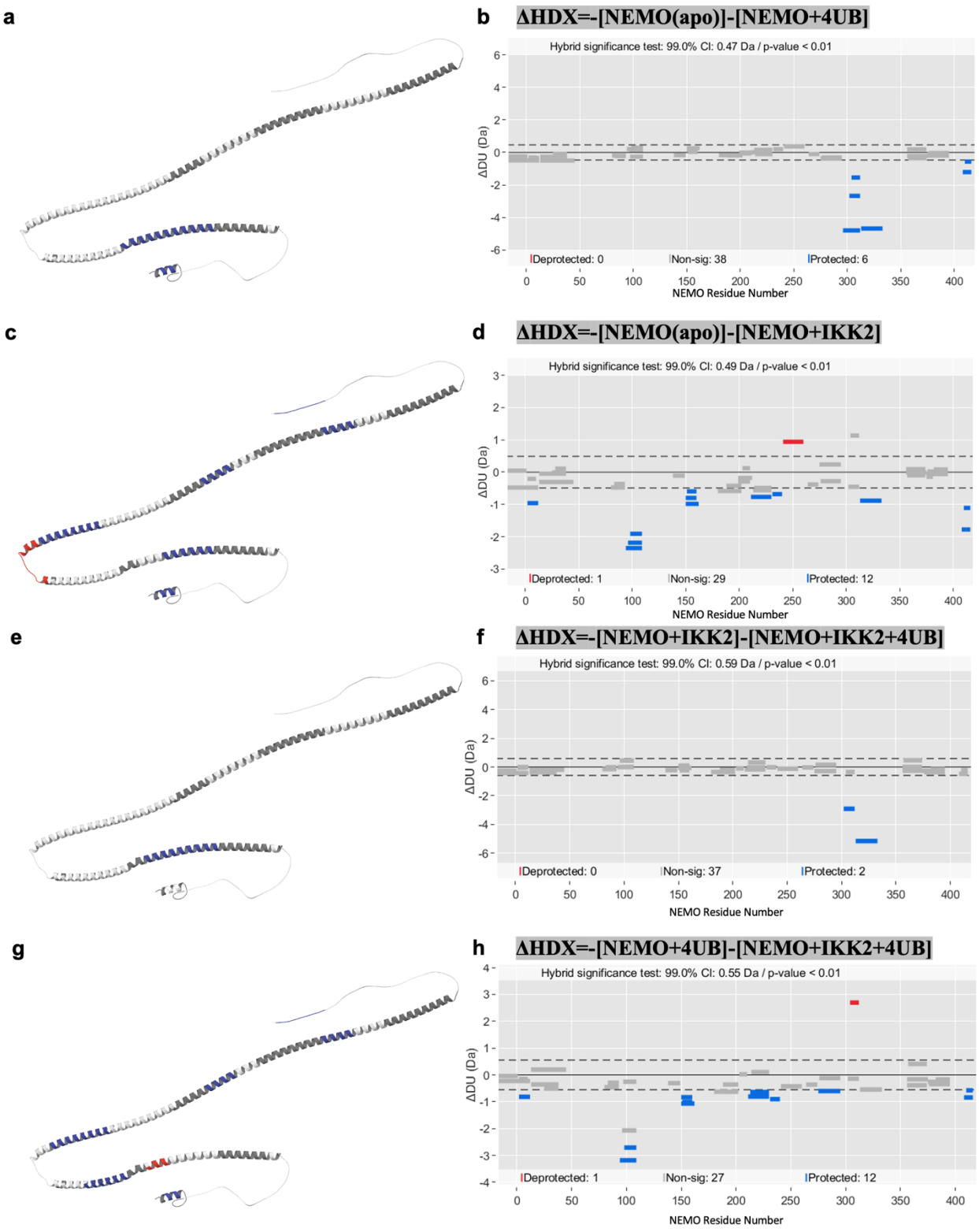

Figure 23. Woods Plots of Statistically Significant Differences in NEMO at 2 minutes. Differences in deuterium uptake at the 2-minute timepoint are plotted in a 2-dimensional Woods plot where peptides are represented by small bars. Blue peptides indicate a statistically significant protection event, gray are non-significant, and red are deprotection events.

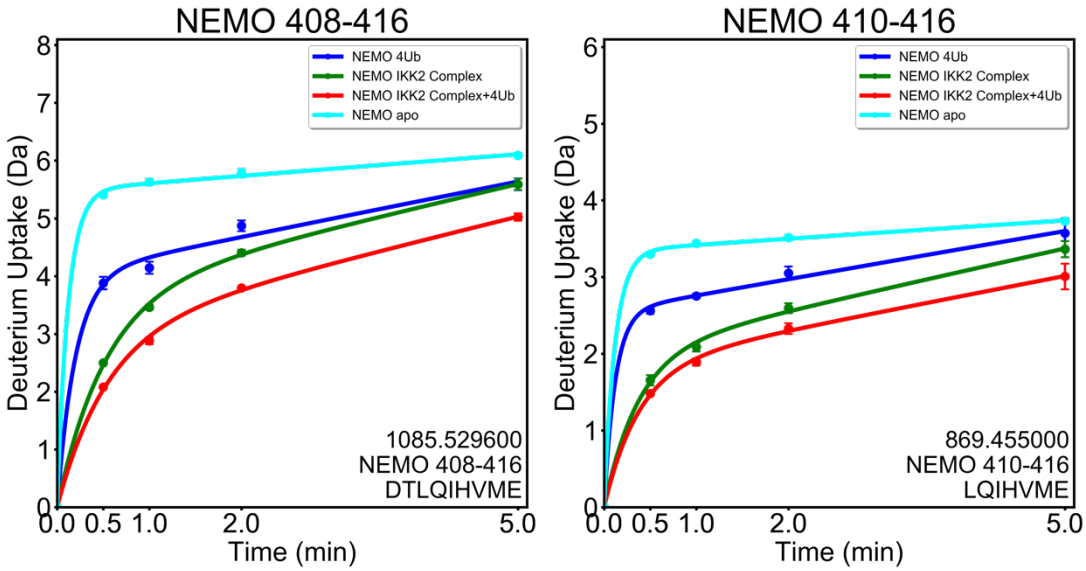

Figure 24. Uptake Plots of the Zinc-Finger Domain. Deuterium incorporation for two overlapping peptides 408-416 (left) and 410-416 (right) across all four timepoints for all four states.

Multiple regions of NEMO undergo structural alteration upon binding to IKK2 and Ub_4

HDX-MS was carried out on NEMO to investigate changes in protein structure and dynamics upon binding to IKK2, Ub_4 and both. To highlight these changes, HDX differences were mapped onto existing structures from the AlphaFold protein structure database. Two styles of interpretation are presented. The first style presents the data "as is" without statistical filtering. Colored structures represent the data without bias, but interpretation of significance can become rather subjective. The second style presents the data after robust statistical filtering. Only peptides that are considered statistically different are colored and highlighted using a predefined significance level. Further information about statistical significance is outlined in Deuteros 2.0 [31].

In Figure 21, differences are plotted using the first style on a relative scale, where blue colors indicate regions where binding of a partner decreases the overall HDX and "protects" NEMO while red colors indicate a region of NEMO that is further exposed upon binding. The differences between states were also illustrated using the statistical approach in Figure 22, where the HDX differences were mapped onto the same existing structure using an absolute scale of red, white, or blue. Using a hybrid significance test to determine statistically significant differences, changes were highlighted directly on the structure and in a 2D Woods plot. Woods plots show all peptides represented as small bars. Gray bars indicate non-significance, blue bars indicate a region of protection, and red bars indicate a region of deprotection going from state 1 to state 2. The same coloring pattern is used in the mapped structures. In examining these HDX differences, multiple significant changes are observed in NEMO in context of its binary and ternary complexes. Some inconsistences in apparent differences arise when examining both styles of data representation.

Binary complexes of NEMO: NEMO shows significant protection in UBAN in a stretch of residues from 296-333 upon exposure to Ub_4 (Fig. 22a-b). Additionally, a region of the Zinc finger domain at the C-terminus shows protection as well from residues 408-416, suggesting that the Zinc finger may bind directly to ubiquitin. These protection data are consistent with previous reports that both the UBAN and the ZFD of NEMO interact with ubiquitin. It is likely that two of the ubiquitin moieties bind to UBAN as previously described and the additional third and fourth Ub moieties interact with the ZFD of NEMO. What is unclear is whether a single Ub moiety interacts with both ZFDs of the NEMO dimer or if two different Ub moieties each interact symmetrically with the ZFDs. A limitation of this method is in detecting such a redundancy.

Binding of IKK2 to NEMO results in the protection of various regions of NEMO as well (Fig. 17c-d). These regions include amino acid residues 2-12, 94-109, 150-162, 211-240, 313-333, and 408-416. Interestingly, a small region spanning residues 241 to 260 which precedes the UBAN domain shows deprotection. Barring segments 94-109 and 150-162, any involvement of the other regions of NEMO in IKK2 binding has not been previously described. Previous mapping experiments between IKK2 and NEMO showed that NEMO with a N-terminal 110 residue deletion cannot bind to IKK2 to any measurable extent, implicating its necessity for binding. However, it was shown that the affinity of NEMO 1-110 for IKK2 was significantly lower than that of NEMO 1-196. Taken together, these observations suggest that participation of the 150-162 segment in IKK2 binding is induced by binding of 1-110 segment. Whether protections of the other four regions result from direct binding or simply refer to dynamic changes in NEMO upon IKK2 engagement is unclear. It is likely that while some of the contacts are affinity enhancers, others are affinity reducers and that their sum contribution is negligible.

Exposure of the 241-260 segment falling near the protected segment further suggests dynamic changes in the structure of NEMO upon IKK2 binding.

Ternary complex of NEMO: Changes in the dynamics of the IKK2:NEMO:Ub_4 complex are estimated by comparison of the binding of Ub_4 to the NEMO:IKK2 complex as well as comparing the ternary state of NEMO:IKK2+Ub_4 to the Ub-bound NEMO. Binding of Ub_4 to a NEMO:IKK2 complex yields protection only in UBAN, which is nearly identical to binding of Ub_4 to apo NEMO. The previously observed ZFD interaction is not statistically significant in this experiment, although it is marginally detectable (Fig. 21). In considering IKK2's effect on NEMO when in the presence of Ub_4, protection of four N-terminal regions (2-12, 94-109, 150-162, and 211-240) as discussed previously remain nearly identical. However, protection and deprotection patterns change in the C-terminal part of NEMO in the ternary complex. The segment encompassing residues 241-260 is no longer deprotected. Instead, a new segment undergoes deprotection (305-315) and another region becomes protected (275-295) (Fig. 22g-h). Some differences arise in the ubiquitin-binding region as well. It should be noted that the deprotected region (305-315) is also deprotected when IKK2 binds NEMO without Ub_4, but the difference is considered statistically non-significant. This is likely due to the HDX per amino acid of the peptide being rather small in the binary complex. A shorter overlapping peptide, had there been one in that region, would likely suggest this region is significant in both cases.

NEMO dynamics in the zinc-finger domain

The Woods plot generated based on the uptake differences at 2 min failed to fully capture the dynamic nature of NEMO binding to IKK2 and Ub_4. For instance, Ub_4 protects both the UBAN and the zinc finger domain. This protection is no longer apparent when Ub_4 is added to

the IKK2:NEMO binary complex. However, clear protection of the zinc finger domain is apparent when both IKK2 and Ub_4 are present (Fig. 24). NEMO 25-38 segment is partially protected in the presence of both IKK2 and Ub_4. This observation suggests that the Ub_4 moieties may contact the N-terminal region of NEMO and this binding is enhanced and possibly induced by NEMO's association with IKK2. Woods plot also reveals that the protection of the Zn-finger motif by IKK2 and Ub_4 is not competitive but additive. That is, the protection is enhanced when both IKK2 and Ub_4 are present. Another NEMO peptide shows protection only at a longer time and in the presence of both Ub_4 and IKK2. This peptide, spanning residues 375 to 395 is particularly significant since our lab recently reported this segment interacts with IKK2 only in the presence of a linear poly ubiquitin chain. More importantly, Ub-dependent interaction of 375-395 with IKK2 is essential for IKK2 activation.

E. HDX-MS of IKK2

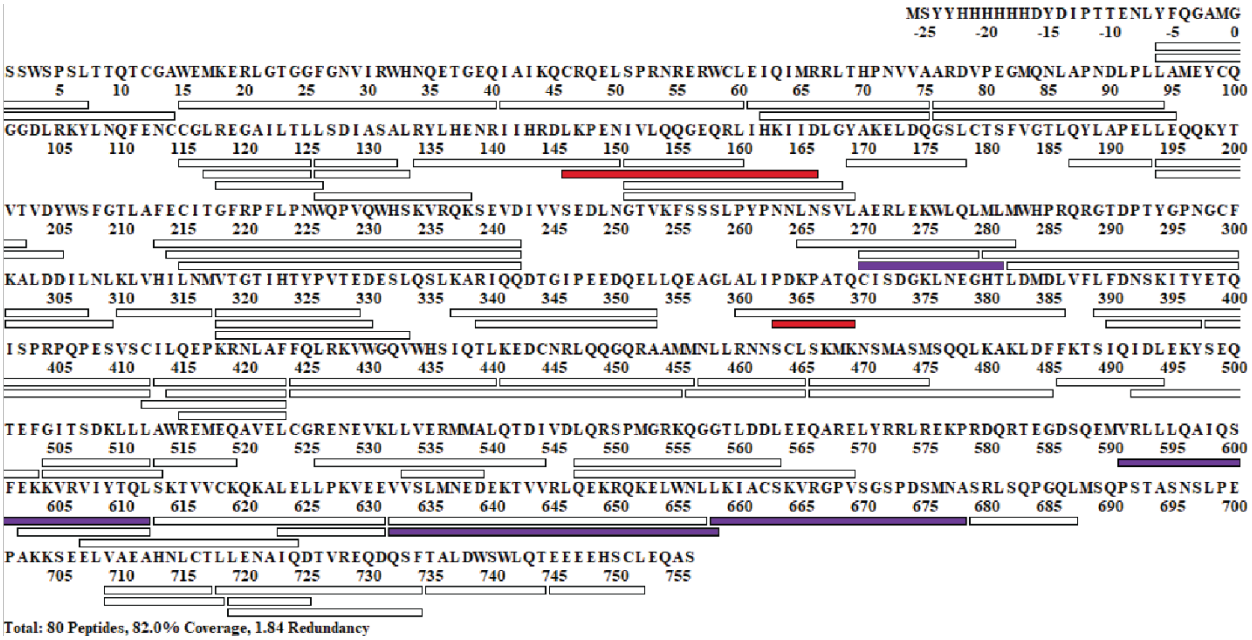

Figure 25: Peptide Coverage Map of IKK2. Peptides colored in white were detected in all conditions. Peptides colored in red were not detected for the IKK2+Ub4 state but were detected in all three other states. Peptides colored in purple were detected for apo IKK2 and NEMO:IKK2 but were not detected in the presence of Ub4 states.

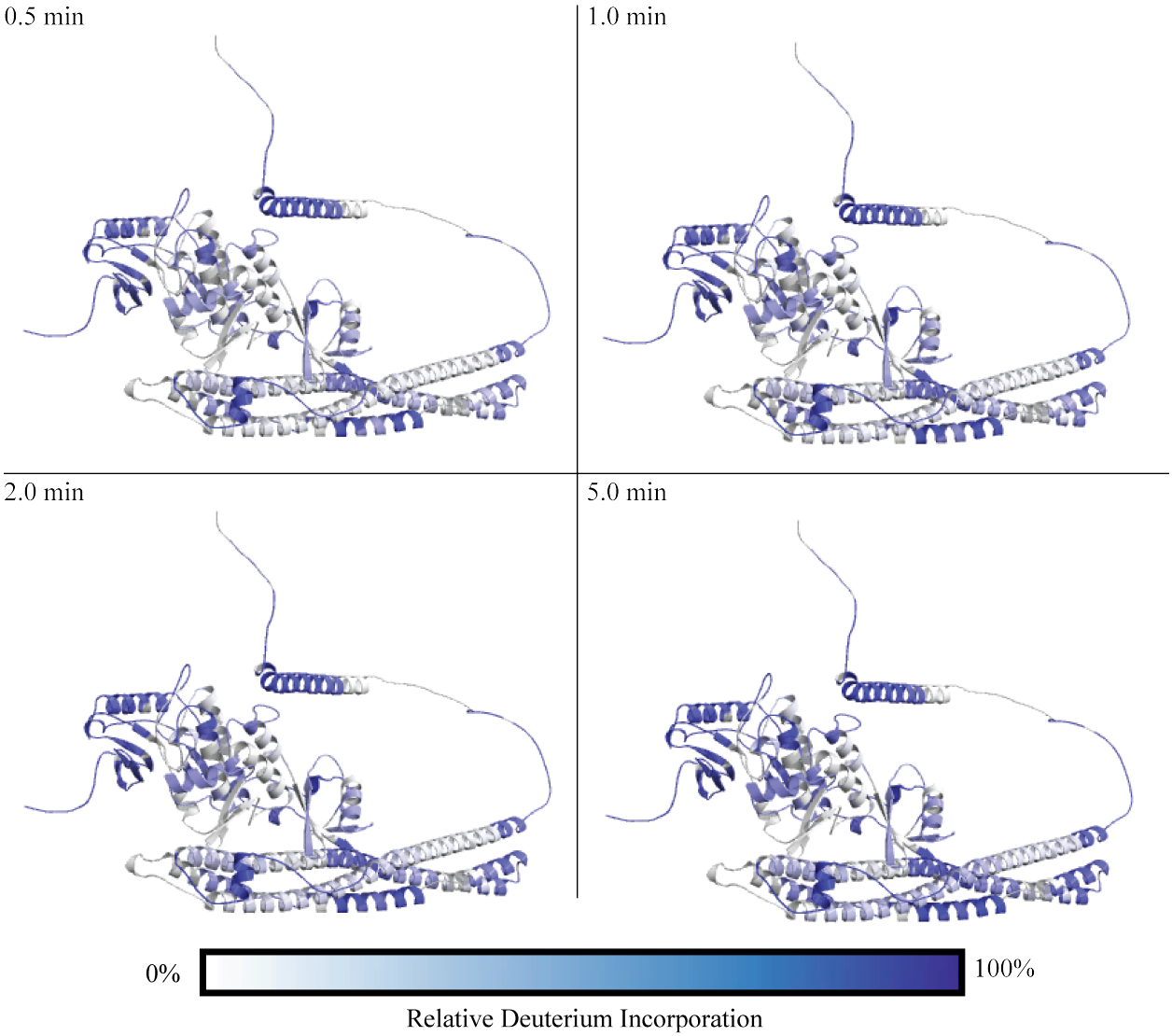

Figure 26: Apo IKK2 HDX. The incorporation of deuterium across IKK2 protein is mapped onto a predicted structure using a full-range scale of relative deuterium uptake. Data from all four timepoints are separately shown in each quadrant and denoted by labeling time. Regions are colored on a gradient scale where increasing intensity of blue indicates greater deuterium incorporation.

IKK2 is a highly structured kinase with multiple flexible regions

IKK2 displays a higher resistance to solvent deuterium exchange than NEMO, as many of its secondary structures remain <50% deuterated even by the 5-minute timepoint. The C-terminal half of the KD as well as the two unbroken helixes of the SDD from 424-494 and 589-658 remain relatively resistant to HDX, save for a small stretch in the first SDD alpha helix from 457-475 that displays higher HDX than the rest of the helix. Regions that exhibit relatively fast deuterium exchange are colored red. These regions include the N-terminal half of the KD (although a small patch is missing coverage in the activation loop), a loop in the ULD from 364-369, the linker between the ULD to the SDD (390-421), the loop between two of the main helixes of the SDD from 497-510, and the entirety of the NBD and SRR starting from residue 659 of the SDD. 18% of the protein sequence lacked coverage, as peptides were either not detected in those regions or the detected peptides did not provide reliable signals.

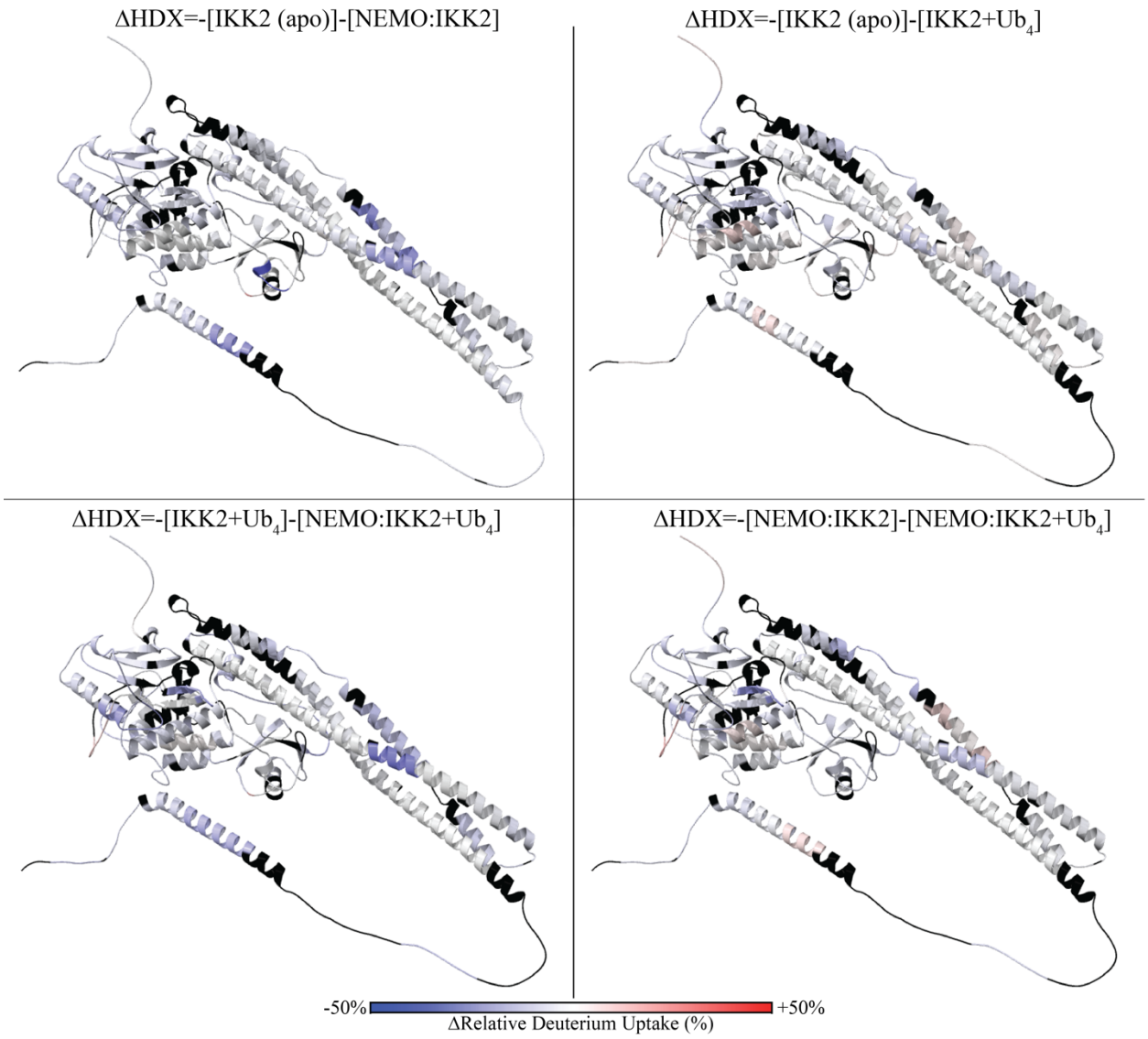

Figure 27: Differential HDX of IKK2 at 5-minute timepoint. Differences in deuterium uptake between two experimental conditions (states) are mapped onto IKK2 structures as ΔHDX = -[State 1] - [State 2]. To maintain a consistency with other illustrations, regions that are colored blue are those in which deuterium uptake in state 2 is less than that of state 1, indicating a protective effect. Regions that are white are non-different between the two states and regions that are red have greater deuterium incorporation in state 2 than in state 1.

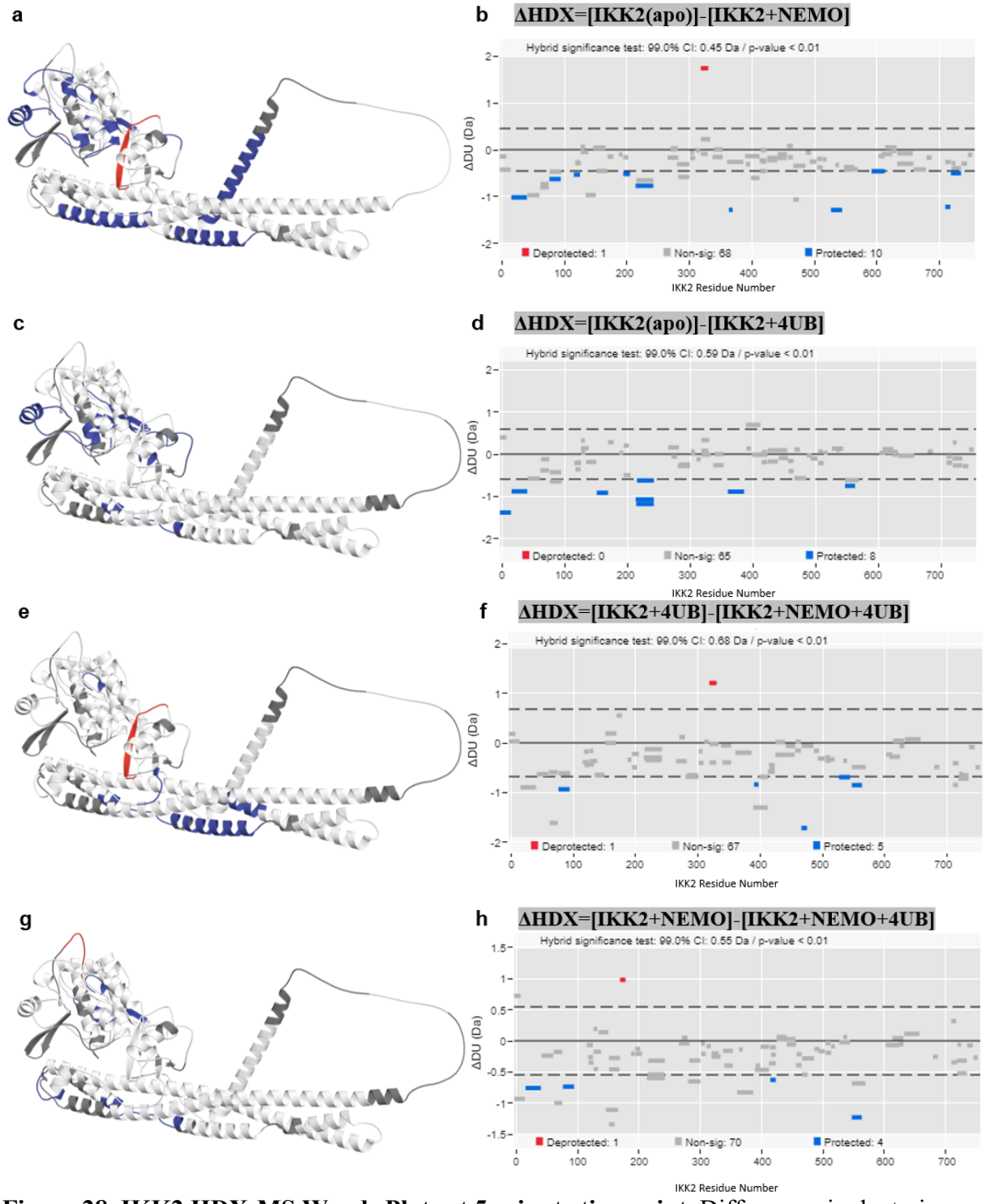

Figure 28. IKK2 HDX-MS Woods Plots at 5-minute timepoint. Differences in deuterium uptake are plotted in a 2-dimensional Woods plot where peptides are represented by small bars. Blue peptides indicate a statistically significant protection event, gray bars are non-significant peptides, and red bars are deprotected regions.

Ub4-bound NEMO, but not NEMO or Ub_4, induces a conformational change in the kinase domain of IKK2 that exposes the activation loop and critical serine residues

Figures 26 and 27 depict changes in IKK2 upon exposure to NEMO, Ub_4 and NEMO+ Ub_4. Woods plots show differential uptake in different parts of the molecule upon oligomerization with NEMO and exposure to Ub_4. Uptake differences in the two areas are consistent with the current knowledge of how IKK2 and NEMO stably associate with other and how it undergoes activation upon binding to linear poly Ub-chains, validating the experimental approach. The first is the protection of the IKK2 segment spanning residues 709 to 734 upon binding to NEMO (Fig. 27a-b) which is known to be responsible for high affinity binding to the N-terminal kinase binding domain of NEMO. The addition of Ub_4 does not induce any additional protection. The second is the activation loop of IKK2 which spans residues 170 to 190. Upon engagement with NEMO+ Ub_4, this segment undergoes deprotection. Not many changes (protection or deprotection) in this segment occur when IKK2 binds independently to Ub_4 or NEMO. This Ub_4-dependent exposure of the activation loop of IKK2 of the IKK2:NEMO complex explains the mechanism of IKK2 activation. Opening of the highly flexible loop allows an active IKK2 or another active kinase to phosphorylate Ser^{177} and Ser^{181} within the loop.

IKK2 dynamics in the IKK2:NEMO complex: In addition to the protection of the NBD by KBD as described above, several other regions of IKK2 also undergo changes upon binding to NEMO. Most of them are located within the kinase domain (segments 15-40, 76-94, 115-125, 194-205, 214-242. Some notable changes are also seen in ULD (segment 363-369), as well as in the SDD (413-423, 466-475, 526-544, 591-612. Only one segment located in the ULD (segment 318-330) exhibits deprotection upon NEMO oligomerization (Fig. 27e-f).

IKK2 changes upon binding to Ub_4: To test how the linear UB-chain affects the dynamics of IKK2 of the IKK2:NEMO complex, we first tested the uptake difference when IKK2 is exposed to Ub_4 alone as a control. IKK2 and ubiquitin are not known to interact physiologically. This control experiment allows us to properly interpret the Ub_4-dependent effect on the IKK2:NEMO. Incubation of IKK2 with a molar excess of Ub_4 generally yields protective effects in various parts of the protein (Fig. 27c-d). Regions that are seemingly unaffected are the NEMO binding domain and the C-terminal half of the kinase domain. Interestingly, some mild protection is seen in multiple areas of the KD and a small stretch of the SDD from 547-563. A region in the ULD from 360-386 also becomes protected. Exposure of an IKK2:NEMO complex to Ub_4 results in similar IKK2 dynamics except for a very pronounced deprotection event on the activation loop from 169-178. In addition to Ub_4-dependent exposure of the activation loop, three regions of the IKK2 in the IKK2:NEMO complex are protected in the presence of Ub_4, which 67-95, 151-169 and 390-397.

A model of the IKK2 complex: Based on the protection and deprotection maps, and published information about binary interactions between IKK2 and NEMO, and between NEMO and Ub_4, we proposed a model for how IKK2 activation occurs as a consequence of Ub_4 binding to NEMO.

IV. Discussion

A. In vitro interaction of IKK2 and NEMO

Investigation of the architectural dynamics of IKK2 and NEMO proteins during assembly first requires confirmation of their interaction and formation of a stable oligomer. Size-exclusion chromatography performed in previous studies showed that NEMO behaves aberrantly in solution and elutes at higher apparent molecular weights than its actual mass. In this study, NEMO behavior was consistent with previous findings and displayed the propensity to form a higher molecular weight complex in the presence of IKK2 (Fig. 17). Comparing the elution profiles of IKK2 and NEMO, NEMO likely exists predominantly as a dimer. Examination of HDX-MS spectra suggested that only one population of NEMO was present in these experiments.

Confirmation of a stable complex in the combined SEC run via SDS-PAGE suggests that IKK2 and NEMO form a stable complex *in vitro*, although it is not obvious to what extent oligomerization has occurred. Because the concern in isolating the IKK2:NEMO complex is that it is both stable and homogenous in oligomeric state, HDX-MS experiments were conducted the same day as sample preparation after size-exclusion chromatography. Performing HDX the same day as sample preparation mitigates any potential protein degradation. A secondary check of homogeneity was also seen in the mass spectra, as multiple populations and peak widening were not observed.

B. Tetra-Ubiquitin's role in oligomerization and activation

Previously, ubiquitin was shown to be necessary and even sufficient for the activation of IKK2 in cells. *In vitro*, ubiquitin does not appear to bind or interact directly with IKK2. Confirmation of ubiquitin binding to NEMO at the established binding site UBAN was observed in HDX-MS as well as second site of interaction in the ZFD. Examination of IKK2 peptides

from this run suggested that Ub_4 binding to NEMO also induced long-range conformational changes in IKK2 structure. Most notably, the activation loop of IKK2 became further exposed to HDX. A physiological explanation for this observation can be made based on existing models that purport IKK2 activation is possible via trans-autophosphorylation. The proposed model identifies ubiquitin as an inducer of conformational change in IKK2. Ubiquitin first binds NEMO bound to IKK2, and this binding event alters the kinase domain, exposing the activation loop. This long-range conformational change may explain the mechanism by which IKK2 may self-activate. Additional contacts with IKK2 by NEMO's ZFD may also play a key role in this assembly which is now activatable and capable of phosphorylation once active.

C. Statistical Analysis of Significant Peptides

HDX-MS results were "filtered" with a 99% confidence level using the hybrid significance test [31]. In short, the test compares the difference in the deuterium uptake between two states for a given peptide to a threshold value determined by a predefined confidence level. Increasing the confidence level to a maximum of 99% in turn increases the threshold and excludes many peptides such that only peptides with very large deuterium uptake differences are considered significant in this study. This approach was taken to simplify the evaluation and interpretation of the structural changes occurring and highlight only the most significant and apparent changes. Other changes that were not highlighted may have real physiological consequences, but they are not emphasized in this study.

D. Interpretation of HDX-MS

Binding of linear M1-linked ubiquitin to NEMO is a previously described interaction. Specifically, the ubiquitin-binding region was previously defined as the coiled-coil 2 domain spanning from residues 259-360. Binding results in significant protection of a stretch of residues

from contained with the known binding region, both confirming the interaction and suggesting that binding of ubiquitin may not involve the entire previously described domain. Interestingly, an additional region of deprotection is observed in the Zinc-finger domain at the C-terminus of NEMO.

Within IKK2, the entire helix alpha 6 (residues ~590 to 660) does not show any change as free or bound to NEMO, Ub or NEMO+Ub. Most parts, but not the entirety of alpha helix 4 (~428 to 495) also do not show any change. One short segment is dynamic (residues ~460 to 474) which is partially protected from uptake upon binding to NEMO/Ub suggesting that it is a dynamic segment. The entire alpha helix 5 is dynamic (~510 to 580). In crystal structures of IKK2, there is a broken segment in the middle of this helix and the presence of an unstructured segment. This helix was always thought to be more dynamic than the other two helices. The activation loop also shows more uptake than the rest of the protein, which is much clearer in the inactive subunit. Even though baculovirus derived IKK2 is phosphorylated, which likely exposes the activation loop, this segment still shows an increase in deuterium uptake in the presence of NEMO + Ub_4. This is consistent with the experimental observation that IKK2 activation requires binding of Ub-chain to NEMO.

E. Additional Remarks

Although the highlighted regions derived from peptides in this study are statistically significant, there are other regions with a consistent pattern observed primarily in IKK2 peptides that were omitted to avoid complication of its discussion. Protein regions that are visibly different in mapped structures sometimes fail to pass the statistical filter. Many of these peptides suggest that additional regions of IKK2 not previously mentioned are possibly physiologically

significant in the discussion of the structural dynamism of IKK2. However, these peptides were not emphasized to simplify the discussion of such a large protein complex.

REFERENCES

[1] Ghosh, G., Wang, V.Y., Huang, D.B., and Fusco, A.J. (2012). NF-κB regulation: Lessons from structures. *Immunological Reviews*, 246, 36-58.

[2] Ghosh, G. and Wang, V.Y. (2021). Origin of the Functional Distinctiveness of NF-κB/p52. *Frontiers in Cell and Developmental Biology*, 9, 764164.

[3] Fusco, A.J., Huang, D.B., Miller, D., Wang, V.Y., Vu, D., and Ghosh, G. (2009). NF-kappaB p52:RelB heterodimer recognizes two classes of kappaB sites with two distinct modes. *EMBO Reports*, 10, 152-159.

[4] Ghosh, S. and Hayden, M.S. (2012). Celebrating 25 years of NF-κB research. *Immunological Reviews,* 246, 5-13.

[5] Sen, R. and Baltimore, D. (1986). Multiple nuclear factors interact with the immunoglobulin enhancer sequences. *Cell Press*, 46, 705-716.

[6] Shih, V.F., Tsui, R., Caldwell, A., and Hoffmann, A. A single NFκB system for both canonical and non-canonical signaling. (2011). *Cell Reports*, 21. 86-102.

[7] Baud, V. and Collares, D. Post-Translational Modifications of RelB NF-κB Subunit and Associated Functions. (2016). *Cells*, 5, 22.

[8] Oeckinghaus, A. and Ghosh, S. The NF-kappaB family of transcription factors and its regulation. (2009). *Cold Spring Harbor Perspectives in Biology*, 1(4): a000034.

[9] Aggarwal, B.B., Takada, Y., Shishodia, S., Gutierrez, A.M., Oommen, O.V., Ichikawa, H., Baba, Y., and Kumar, A. (2004). Nuclear transcription factor NF-kappa B: role in biology and medicine. *Indian Journal of Experimental Biology*, 42, 341-353.

[10] Karin, M. and Delhase, M. The I kappa B kinase (IKK) and NF-kappa B: key elements of proinflammatory signalling. (2000). *Seminars in Immunology*, 12, 85-98.

[11] Xiao, G., Harhaj, E.W., and Sun, S.C. NF-κB-inducing kinase regulates the processing of NF-κB2 p100. (2001). *Molecular Cell*, 7, 401-409.

[12] Yu, H., Lin, L., Zhang, Z, and Hu, H. Targeting NF-κB pathway for the therapy of diseases: mechanism and clinical study. (2009). *Signal Transduction and Targeted Therapy*, 5, 209.

[13] Miller, B.S. and Zandi, E. Complete reconstitution of human IκB kinase (IKK) complex in yeast. (2001). *The Journal of Biological Chemistry*, 276, 36320-36326.

[14] Israël, A. The IKK complex, a central regulator of NF-kappaB activation. (2010). *Cold Spring Harbor Perspectives in Biology,* 2(3): a000158.

[15] Li, Q., Van Antwerp, D., Mercurio, F., Lee, K.F., and Verma, I.M. Sever liver degeneration in mice lacking the IkappaB kinase 2 gene. (1999). *Science,* 284, 321-325.

[16] Li, Z.W., Chu, W., Hu, Y., Delhase, M., Deerinck, T., Ellisman, M., Johnson, R., and Karin, M. The IKKβ subunit of IκB kinase (IKK) is essential for nuclear factor κB activation and prevention of apoptosis. (1999). *The Journal of Experimental Medicine*, 189, 1839-1845.

[17] Courtois, G., Smahi, A., and Israel, A. NEMO/IKKγ: linking NF-κB to human disease. (2001). *Trends in Molecular Medicine*¸ 7, 427-430.

[18] Zhang, J., Clark, K., Lawrence, T., Peggie, M.W., and Cohen, P. An unexpected twist to the activation of IKKβ: TAK1 primes IKKβ for activation by autophosphorylation. (2014). *Biochemical Journal*, 461, 531-537.

[19] Shim, J.H., Xiao, C., Paschal, A.E., Bailey, S.T., Rao, P., Hayden, M.S., Lee, K.Y., Bussey, C., Steckel, M., Tanaka, N., Yamada, G., Akira, S., Matsumoto, K., and Ghosh, S. TAK1, but not TAB1 or TAB2, plays an essential role in multiple signaling pathways in vivo. (2005). *Genes and Development*, 19, 2668-2681.

[20] Wajant, H. and Siegmund, D. TNFR1 and TNFR2 in the Control of the Life and Death Balance of Macrophages. (2019). *Frontiers in Cell and Developmental Biology*, 7, 91.

[21] Rahighi, S., Ikeda, F., Kawasaki, M., Akutsu, M., Suzuki, N., Kato, R., Kensche, T., Uejima, T., Bloor, S., Komander, D., Randow, F., Wakatsuki, S., and Dikic, I. Specific Recognition of Linear Ubiquitin Chains by NEMO Is Important for NF-κB Activation. (2009). *Cell*, 136, 1098-1109.

[22] Xu, G., Lo, Y.C., Li, Q., Napolitano, G., Wu, X., Jiang, X., Dreano, M., Karin, M., and Wu, H. Crystal structure of inhibitor of κB kinase β. (2011). *Nature*, 472, 325-330.

[23] Polley, S., Huang, D.B., Hauenstein, A.V., Fusco, A.J., Zhong, X., Vu, D., Schöfelbauer, B., Kim, Y., Hoffman, A., Verma, I.M., Ghosh, G., and Huxford, T. A Structural Basis of IκB Kinase 2 Activation Via Oligomerization-Dependent *Trans* Auto-Phosphorylation. (2013). *The Public Library of Science Biology*, 11(6), e1001581

[24] Jumper, J., Evans, R., Pritzel, A., Green, T., Figurnov, M., Ronneberger, O., Tunyasuvunakool, K., Bates, R., Žídek, A., Potapenko, A., Bridgland, A., Meyer, C., Kohl, S.A.A., Ballard, A.J., Cowie, A., Romera-Paredes, B., Nikolov, S., Jain, R., Adler, J., Back, T., Petersen, S., Reiman, D., Clancy, E., Zielinski, M., Steinegger, M., Pacholska, M., Berghammer, T., Bodenstein S., Silver, D., Vinyals, O., Senior, A.W., Kavukcuoglu, K., Kohli, P., and Hassabis, D. Highly accurate protein structure prediction with AlphaFold. (2021). *Nature*, 596, 583-589.

[25] Zheng, C., Yin, Q., and Wu, H. Structural Studies of NF-κB signaling. (2011). *Cell Research*, 21, 183-195.

[26] Shaffer, R., DeMaria, A.M., Kagermazova, L., Liu, Y., Babaei, M., Caban-Penix, S., Cervantes, A., Jehle, S., Makowski, L., Gilmore, T.D., Whitty, A., and Allen, K.N. A central region of NF-κB essential modulator is required for IKKβ-induced conformational change and for signal propagation. (2019). *Biochemistry*, 58, 2906-2920.

[27] Nolen, B., Taylor, S., and Ghosh, G. Regulation of protein kinases; controlling activity through activation segment conformation. (2004). *Molecular Cell*, 15, 661–675.

[28] Vinciauskaite, V. and Masson, G.R. Fundamentals of HDX-MS. (2022). *Essays in Biochemistry,* EBC20220111.

[29] Masson, G.R., Burke, J.E., Ahn, N.G., Anand, G.S., Borchers, C., Brier, S., Bou-Assaf, G.M., Engen, J.R., Englander, S.W., Faber, J., Garlish, R., Griffin, P.R., Gross, M.L., Guttman, M., Hamuro, Y., Heck, A.J.R., Houde, D., Iacob, R.E., Jørgensen, T.J.D., Kaltashov, I.A., Klinman, J.P., Konermann, L., Man, P., Mayne, L., Pascal, B.D., Reichmann, D., Skehel, M., Snijder, J., Strutzenberg, T.S., Underbakke, E.S., Wagner, C., Wales, T.E., Walters, B.T., Weis, D.D., Wilson, D.J., Wintrode, P.L., Zhang, Z., Zheng, J., Schriemer, D.C., and Rand, K.D. Recommendations for performing, interpreting and reporting hydrogen deuterium exchange mass spectrometry (HDX-MS) experiments. (2019). *Nature Methods,* 16, 595–602

[30] Shaul, J.D., Farina, A., and Huxford, T. The human IKKβ subunit kinase domain displays CK2-like phosphorylation specificity. (2008). *Biochemical and Biophysical Research Communications,* 374, 592–597.

[31] Peacock, R.B., Davis, J.R., Markwick, P.R.L., and Komives, E.A. Dynamic Consequences of Mutation of Tryptophan 215 in Thrombin. (2018). *Biochemistry,* 57, 2694-2703

[32] Wales, T.E., Fadgen, K.E., Gerhardt, G.C., and Engen, J.R. High-speed and high-resolution UPLC separation at zero degrees Celsius. (2018). *Analytical Chemistry,* 80, 6815-6820

[33] Ramsey, K.M., Dembinski, H.E., Chen, W., Ricci, C.G., and Komives, E.A. DNA and IκBα both induce long range conformational changes in NFκB. (2017). *Journal of molecular biology*. 429, 999-1008.

[34] Lumpkin, R.J. and Komives, E.A. DECA, a comprehensive, automatic post-processing program for HDX-MS data. (2019). *Molecular and cellular proteomics*, 18, 2516-2523.

[35] Lau, A.M., Claesen, J., Hansen, K., and Politis, A. Deuteros 2.0: peptide-level significance testing of data from hydrogen deuterium exchange mass spectrometry. (2021). *Bioinformatics*, 37, 270-272.

[36] Berman, H.M., Westbrook, J., Feng, Z., Gilliland, G., Bhat, T.N., Weissig, H., Shindyalov, I.N., and Bourne, P.E. The Protein Data Bank. (2000). *Nucleic Acids Research*, 28, 235-242.

[37] Schrödinger, L., & DeLano, W. (2020). *PyMOL*. Retrieved from http://www.pymol.org/pymol

[38] Adobe Inc. (2019). *Adobe Illustrator*. Retrieved from https://adobe.com/products/illustrator

[39] Ivins, F.J., Montgomery, M.G., Smith, S.J.M., Morris-Davies, A.C., Taylor, I.A. and Rittinger, K. NEMO oligomerization and its ubiquitin-binding properties. (2009). *The Biochemical Journal,* 421, 243–51.

[40] Ko, M.S., Biswas, T., Mulero, M.C., Bobkov, A.A., Ghosh, G., and Huxford, T. Structurally plastic NEMO and oligomerization prone IKK2 subunits define the behavior of human IKK2:NEMO complexes in solution. (2020). *BBA Proteins and Proteomics,* 1868, p. 140256